Journal of Geochemical Exploration 254 (2023) 107310

Contents lists available at ScienceDirect

Journal of Geochemical Exploration

journal homepage: www.elsevier.com/locate/gexplo

Trace element compositions and geochronology of cassiterite from the Bushveld Large Igneous Province, South Africa

Teimoor Nazari-Dehkordi [a,b,*], Xiao-Lei Wang [c], Axel Hofmann [b], Rong-Qing Zhang [c], Laurence Robb [b,d,e], Henriette Ueckermann [b]

[a] School of Earth Sciences, University College Dublin, Belfield, Dublin, Ireland
[b] DSI-NRF CIMERA, Department of Geology, University of Johannesburg, Johannesburg, South Africa
[c] State Key Laboratory for Mineral Deposits Research, School of Earth Sciences and Engineering, Nanjing University, Nanjing 210023, China
[d] School of Geosciences, University of the Witwatersrand, Private Bag 3, 2050 Johannesburg, South Africa
[e] Department of Earth Sciences, University of Oxford, South Parks Road, OX1 3AN Oxford, United Kingdom

ARTICLE INFO

Keywords:
Bushveld Large Igneous Province
Cassiterite
Zaaiplaats
Union Tin Member
Rooiberg Group
Rooiberg Fragment

ABSTRACT

This study presents trace element compositions and ages of four representative cassiterite samples from the Zaaiplaats, Union and Rooiberg Sn fields, all spatially associated with the Bushveld Large Igneous Province (LIP), South Africa. The Zaaiplaats Sn field is endogranitic and entirely hosted within the variably-altered Bobbejaankop and Lease granites of the Lebowa Granite Suite. In contrast, the exogranitic Union and Rooiberg Sn fields occur within the Union Tin Member of the Rooiberg Group, and the Pretoria Group of the Transvaal Supergroup, respectively. Collectively, all the cassiterite samples display quasi-parallel chondrite-normalised rare earth element (REE) patterns characterised by relative enrichments in the heavy REE, and yielded ages varying within a relatively restricted interval between 2061 ± 40 Ma and 2054 ± 3 Ma. This age range compares well with those reported from the Bushveld LIP and, when combined with mineral compositions, suggests a common granitic source for cassiterites from all the Sn fields. The exogranitic Rooiberg and Union Sn fields are identified by cassiterites with Zr/Hf of ~40, whereas the endogranitic Zaaiplaats Sn field is characterised by cassiterites enriched in most incompatible elements (e.g., Nb, Ta, Zr, Hf, In, F and B) and Zr/Hf of ~10. These Zr/Hf ratios agree with the endogranitic and exogranitic Sn ores from other localities, but are different from the very low Zr/Hf ratios of ~3 reported for endogranitic cassiterites associated with rare-metal granites. The Zr versus Hf discrimination diagram may therefore be useful for distinguishing the endogranitic and exogranitic origins of cassiterites and for identifying the extent of fractionation of the causative source.

1. Introduction

The Bushveld Large Igneous Province (LIP) comprises four major rock suites: (1) volcanic rocks of the Rooiberg Group; (2) mafic-ultramafic cumulates known as the Rustenburg Layered Suite (RLS); (3) sub-volcanic granophyric rocks referred to as the Rashoop Granophyre Suite (RGS); and (4) voluminous granitic rocks of the Lebowa Granite Suite (LGS). A substantial amount of research has been carried out on the RLS that contains huge resources of platinum-group elements (PGE), Cr and Fe—Ti (e.g., Barnes et al., 2010 and references therein). In contrast, the felsic rocks of the Bushveld LIP (Rooiberg Group, RGS and LGS), although associated with a variety of ore deposits (e.g., Sn, F, Iron oxide Cu—Au) of varying grade and tonnage, have received much less attention. The origin and evolution of these felsic rocks and associated ores have remained poorly understood. In particular, available literature on the Sn mineralisation associated with the Bushveld LIP is limited to a few decades-old publications. The felsic rocks of the Bushveld LIP and adjacent sedimentary successions of the Transvaal Supergroup host numerous, currently-inactive Sn mines and prospects (Fig. 1; Lenthall, 1974). The rapid increase in demand and price for Sn combined with reports of elevated concentrations of highly sought-after rare earth elements (REE) associated with the Sn fields in and around the Bushveld LIP such as prominent bastnaesite [$Ce(CO_3)F$] mineralisation reported from the Groenvley-Appingendam district of the Zaaiplaats Sn field (Strauss, 1954), have renewed interests in exploration for Sn. However, available data on the trace element compositions and ages of cassiterite

* Corresponding author at: School of Earth Sciences, University College Dublin, Belfield, Dublin, Ireland.
E-mail address: teimoor.nazaridehkordi@ucd.ie (T. Nazari-Dehkordi).

https://doi.org/10.1016/j.gexplo.2023.107310
Received 1 May 2023; Received in revised form 20 August 2023; Accepted 8 September 2023
Available online 11 September 2023

ores from the Bushveld LIP are absent, hindering a detailed understanding of Sn mineralisation in the region.

Tin mineralisation associated with the Bushveld LIP is commonly hosted within, or are spatially associated with, highly-evolved A-type granites of the LGS (Robb et al., 2000). Tin-bearing granites usually record prolonged and extreme fractional crystallisation from intermediate-felsic melts originating from a lower crustal source that experienced a series of magmatic and hydrothermal processes involving melt fractionation, volatile saturation and fluid-rock interactions (Schaltegger et al., 2005). As a result, Sn-bearing granites record varying degrees of mineralisation and alteration, which subsequently limit the applicability of conventional whole-rock geochemistry in the investigation of ore-forming mechanisms. Nonetheless, cassiterite as a tin oxide mineral (SnO_2) of the rutile group and the prime source of Sn worldwide, incorporates a large number of trace elements. This trace-element affinity enables cassiterite to fingerprint fluid compositions and mineralisation processes (Cheng et al., 2019 and references therein). Moreover, cassiterite is a robust U—Pb geochronometer that has provided reliable ages for various Sn deposits of different ages (e.g., Gejiu and Dachang districts of the Youjiang Basin tin province, China: Guo et al., 2018, Cheng et al., 2019; Bolivian tin belt: Gemmrich et al., 2021; Erzgebirge tin province, Germany-Czech Republic: Zhang et al., 2017a; Karagwe-Ankole tin belt, Rwanda: Nambaje et al., 2021; Yazov granite, Eastern Siberia: Neymark et al., 2021).

This study presents trace element compositions and ages of representative cassiterite samples from three major Sn fields of the Bushveld LIP including the Zaaiplaats, Union and Rooiberg districts. These datasets are used to directly define the timing of Sn mineralisation and constrain the mechanisms responsible for the incorporation of trace elements into the cassiterite structure. In particular, Zr/Hf ratios of the Bushveld cassiterites are compared with an existing dataset from other Sn occurrences worldwide and used as a proxy to identify degrees of fractionation as well as rare-metal potential of causative sources.

2. Geological setting

A large number of publications have discussed various geological aspects of the Bushveld LIP (e.g., Cawthorn and Walraven, 1998; Zeh et al., 2015). In brief, the Bushveld LIP appears in the Kaapvaal Craton, the southern part of the Kalahari Craton (Fig. 1a), and is bounded by multiple crustal-scale shear zones such as the Thabazimbi-Murchison Lineament, the Zoetfontein-Palala Shear Zone and the Triangle Shear Zone (Fig. 1b), which resulted from the pre-Bushveld assemblage of the Witwatersrand Block, the Pietersburg Block, the Limpopo Belt Central Zone and the Zimbabwe Craton between ~2.97 Ga and ~2.65 Ga (e.g., Laurent et al., 2014; Zeh et al., 2015). The Bushveld LIP consists of ~555,000 km^3 of mafic-ultramafic and ~600,000 km^3 of felsic rocks (Hill et al., 1996; Cawthorn and Walraven, 1998) which collectively

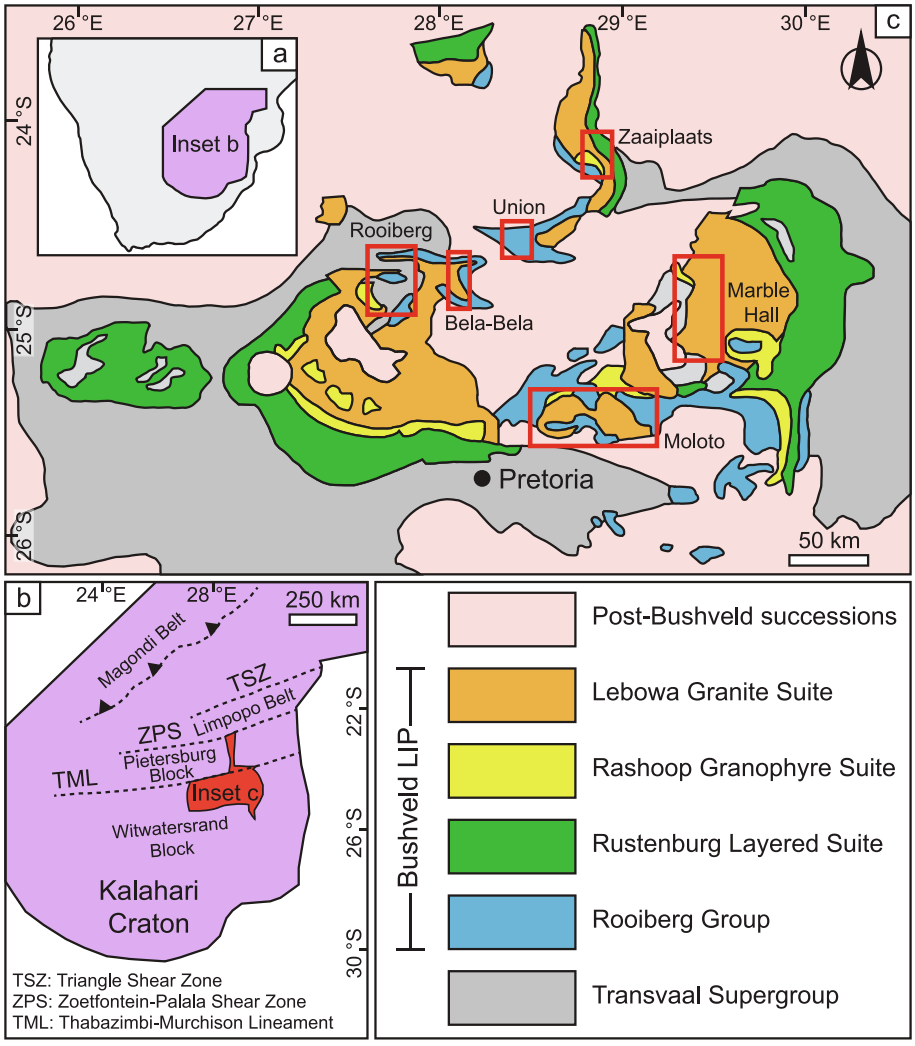

Fig. 1. (a) Geographical location of the Kalahari Craton in Southern Africa; (b) Geographical location of the Bushveld Large Igneous Province (LIP) in the Kalahari Craton; (c) Simplified geological map of the Bushveld LIP and associated Sn fields. Insets a-c are modified after Zeh et al. (2015).

form the eastern, western, far western, northern and south-eastern limbs (Fig. 1c). Inferences on the origin of the Bushveld LIP are provided below.

2.1. Rooiberg Group

The Rooiberg Group, recording the earliest magmatic activity associated with the Bushveld LIP, overlies the Transvaal Supergroup and consists of ~3500 m of lavas and subaerial pyroclastic rocks with sedimentary interlayers. The Rooiberg Group covers an area of ~300,000 km^3 and is divided into four formations, in ascending stratigraphic order, the Dullstroom, Damwal, Kwaggasnek and Schrikkloof formations (Schweitzer et al., 1995). The ~1500 m-thick Dullstroom Formation consists of a differentiated suite ranging from basalt to rhyolite and is intruded by the mafic-ultramafic rocks of the RLS. The Dullstroom Formation is overlain by the Damwal, Kwaggasnek and Schrikkloof formations, which are composed largely of dacite and rhyolite (Schweitzer et al., 1995). The Dullstroom Formation reflects partial melting of a mafic lower crustal source, whereas the silica-rich Damwal, Kwaggasnek and Schrikkloof formations represent a fractionally crystallised melt with an intermediate composition (Nazari-Dehkordi and Robb, 2022a).

2.2. Rustenburg Layered Suite

The mafic-ultramafic sequences of the RLS consist of five major lithological zones. These include the Marginal Zone (mafic and ultramafic sills and dykes, Sharpe, 1981), the Lower Zone (harzburgite-pyroxenite), the Critical Zone (norite, pyroxenite, anorthosite and intercalated chromitite as well as PGE-rich layers, Cawthorn et al., 2006), the Main Zone (anorthosite, norite, gabbronorite), and the Upper Zone (anorthosite, magnetitite, gabbronorite, Barnes et al., 2010).

2.3. Rashoop Granophyre Suite

The shallow intrusive granophyric rocks of the RGS occur as sill-like bodies in contact with the RLS, LGS and Rooiberg Group, and are divided into the Stavoren and Diepkloof granophyres and the Zwartbank Pseudogranophyre (Walraven, 1985, 1987). The Stavoren Granophyre is the most common variety that largely appears in-between the Rooiberg volcanics and the LGS, and represents a shallow intrusive counterpart of the upper Rooiberg Group (Walraven, 1987) or a residual melt from the RLS (Mathez et al., 2013; Skursch et al., 2020). The Diepkloof Granophyre and Zwartbank Pseudogranophyre occur between the RLS and the Rooiberg volcanics, and between the RLS and the Transvaal Supergroup, respectively. These are regarded as melts of the Rooiberg volcanics and the Transvaal Supergroup, generated after the emplacement of the RLS (Walraven, 1987).

2.4. Lebowa Granite Suite

The ~1500 m-thick granitic sheets of the LGS represent the youngest intrusive event associated with the Bushveld LIP and include a number of tabular bodies with limited variation in mineralogy and texture (Fig. 1c), which collectively occupy an area of ~50,000 km^2, with an estimated volume of ~205,000 km^3 (Kleemann and Twist, 1989; Hill et al., 1996). In most parts, the LGS overlies the mafic-ultramafic rocks of the RLS and is in turn overlain by the Rooiberg Group and RGS. In the well-exposed areas of the eastern limb, the LGS develops a gradational contact with the Stavoren-type RGS (Hill et al., 1996). Moreover, Skursch et al. (2020) reported that the granitic and mafic-ultramafic magmas that generated the LGS and RLS, respectively, partly coexisted. Collectively, the parental magma of the granitic rocks of the LGS was generated under water-poor (anhydrous) conditions as an unusually hot magma (≥900 °C) as expected for typical A-type granites (Kleemann and Twist, 1989; Robb et al., 2000).

The LGS is associated with a large number of magmatic-hydrothermal ore deposits (Robb et al., 2000; Crocker et al., 2001) that are hosted within the granitic rocks (e.g., Zaaiplaats Sn mine) or in the nearby rock horizons such as the RGS, Rooiberg Group and the sedimentary layers of the Transvaal Supergroup. These orebodies resulted from a three-stage paragenetic sequence including an early magmatic-hydrothermal Sn—W (±Mo-F) ore, an intermediate hydrothermal Cu-Pb-Zn (±As-Ag-Au) orebody and late-stage hydrothermal Fe (±F-U) mineralisation events (Robb et al., 2000).

3. Tin mineralisation associated with the Bushveld LIP

The Bushveld LIP contains numerous now-defunct Sn mines and prospects of variable size and grade, which geographically form six discernible Sn fields (Lenthall, 1974). These include the Zaaiplaats, Rooiberg, Union (also known as Nylstroom), Bela-Bela (also known as Elands and Warmbaths), Marble Hall (also known as Stavoren-Mute Fides and Olifants) and Moloto Sn fields (Fig. 1c), of which the Zaaiplaats and Rooiberg Sn fields were the most important and economically viable. The Sn mineralisation appears largely in the granitic rocks of the LGS and the sedimentary successions of the Transvaal Supergroup and, to a lesser extent, within the volcaniclastic horizons of the Rooiberg Group and the granophyric rocks of the RGS. The present study focuses on the Zaaiplaats (granite-hosted, i.e. endogranitic ore), Union (exogranitic ore hosted in the Rooiberg Group) and Rooiberg (exogranitic ore hosted in the Transvaal Supergroup) Sn fields.

3.1. Zaaiplaats Sn field

The Zaaiplaats Sn field occurs in the northern limb of the Bushveld LIP and is entirely hosted by the granitic rocks of the LGS. In this area, the LGS is represented by the cogenetic Nebo, Bobbejaankop and Lease granites (Fig. 2a). The Sn mineralisation is limited to the Bobbejaankop and Lease granites. Petrographic and geological aspects of these granites are discussed in detail elsewhere (e.g., Pollard et al., 1991; McNaughton et al., 1993; Nazari-Dehkordi and Robb, 2022b).

The tabular sheet of Nebo granite is coarse-grained, unaltered and barren. It consists mainly of quartz, plagioclase, perthitic alkali-feldspar and hornblende, with a hornblende-rich lower part and biotite-bearing upper part, reflecting fractional crystallisation of a single magma (e.g., Kleemann and Twist, 1989). The coarse-grained Bobbejaankop granite exhibits gradational contacts with the underlying Nebo and overlying Lease granites. The Bobbejaankop and Lease granites are both red-coloured, composed of quartz, alkali feldspar, chlorite and epidote, the latter two replacing biotite and minor magnetite. The up to 150 m-thick fine-grained Lease granite is a lenticular sheet-like body that intrudes into the overlying granophyric rocks of the RGS (Strauss, 1954). The Bobbejaankop and Lease granites are extensively altered, as indicated by the replacement of biotite by chlorite, epidote and sericite, and partial to complete replacement of alkali feldspar by chlorite and sericite. Miarolitic cavities are abundant, particularly in the Lease granite, and contain quartz and alkali feldspar, and minor fluorite, chlorite, albite, sericite and calcite. Cavities associated with the orebodies additionally contain minor cassiterite, scheelite ($CaWO_4$), bastnaesite and synchysite [$CaCe(CO_3)_2F$]. Although variable in size, these infilling hydrothermal minerals usually appear as coarse-grained crystals up to 5 cm-long with a pegmatitic texture (McNaughton et al., 1993).

The Nebo granite is regarded as the product of partial melting of a lower crustal source that potentially incorporated metasedimentary components (Zirakparvar et al., 2019). The Nebo magma, however, further evolved into a highly-fractionated melt enriched in fluids, volatiles and incompatible trace elements from which the Sn-bearing Bobbejaankop and Lease granites were derived (McNaughton et al., 1993; Robb et al., 1994).

The Zaaiplaats Sn mineralisation, described in detail in Pollard et al. (1989, 1991), appears in three major styles, as illustrated schematically

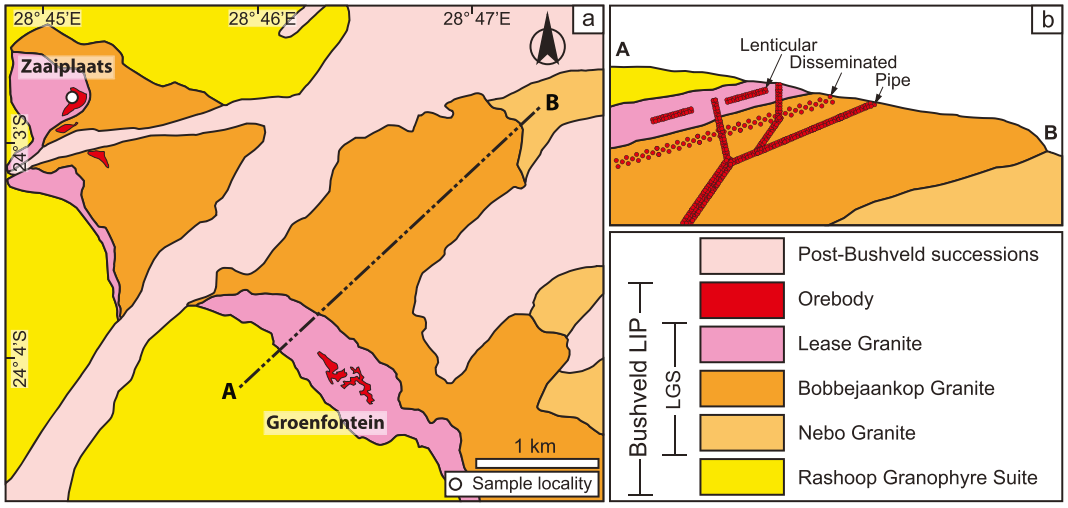

Fig. 2. (a) Geological map of the Zaaiplaats Sn field surrounding the Zaaiplaats and Groenfontein Sn mines; (b) A schematic cross-section (A–B) showing various granitic rocks and associated styles of Sn mineralisation. Insets a–b are modified after Coetzee (1984).

in Fig. 2b: (1) Disseminated mineralisation is characterised by a gently west-dipping, crescent-shaped horizon in the Bobbejaankop granite (Coetzee, 1984), along which the cassiterite ore appears as coarse-grained euhedral crystals replacing quartz, and in a close association with chlorite and sericite replacing biotite, and also within the miarolitic cavities as a fine-grained infilling mineral associated with quartz and feldspar. (2) Lenticular, sub-horizontal and tabular orebodies in the Lease granite are up to 10 m-thick with up to 70 % cassiterite, and are characterised by a halo of intense hydrothermal alterations. The cassiterite ore appears in miarolitic cavities as an infilling hydrothermal mineral and as a partial replacement of alkali feldspar in association with fine-grained sericite, chlorite, pyrite, fluorite and tourmaline. (3) A number of localised, shallowly NW-plunging, inter-linked ore-bearing pipes occur exclusively in the Lease and Bobbejaankop granites (Strauss, 1954; Pollard et al., 1991). There are multiple generations of pipes with considerable variations in plunge and strike, and diameters ranging from <10 cm to 10 m, and lengths ranging from <10 m to >900 m. The mineralised pipes are characterised by an outer zone filled largely with fine-grained quartz and radiating tourmaline aggregates and an inner zone composed mainly of a mineralised, fine-grained granite displaying various degrees of alteration, dissolution and infilling by euhedral cassiterite, feldspar, sericite, chlorite, fluorite and calcite.

Most cassiterite-bearing pipes are vertical or steeply inclined and characterised by a shallow part rich in cassiterite representing lower temperatures, and a deeper part corresponding to higher temperatures that preferentially stabilise tourmaline and other relatively high-temperature minerals (Strauss, 1954). These steeply-plunging pipes represent an upward migration of volatile-rich fluids during which hydrothermal minerals partly or completely replaced the Lease and Bobbejaankop granites (e.g., Strauss, 1954; Pollard et al., 1989). In contrast, the pipes concordant with the transitional boundary between the Lease and Bobbejaankop granites originated from volatile-rich fluids released from a gradually-solidifying magma that subsequently moved along partially-crystallised portions. These concordant pipes usually occur at deep levels and are associated with higher temperatures unfavourable for the formation of cassiterite (Strauss, 1954).

Gulson and Jones (1992) published an age of 2099 ± 3 Ma for a cassiterite sample from the Zaaiplaats Sn field using isotope-dilution thermal ionisation mass-spectrometry (ID-TIMS). However, this age is considered inaccurate due to difficulties related to incomplete dissolution of cassiterite (Neymark et al., 2018).

3.2. Union Sn field

The Union Sn field is characterised by low-grade Sn mineralisation that produced nearly 11,000 tons of Sn concentrate during intermittent mining operations from 1909 until 1983 (Strauss, 1954; Menge, 1963). The Sn mineralisation is restricted to the Union Tin Member of the Rooiberg Group, intercalated between the rhyolites of the underlying Kwaggasnek and overlying Schrikkloof formations, which are unconformably overlain by the sedimentary successions of the Waterberg Group (Fig. 3). Granitic outcrops displaying characteristics comparable to the Nebo (unaltered) and Bobbejaankop (altered with miarolitic cavities) granites have also been reported from the Union Sn field (Crocker et al., 2001). The Union Sn field is located along the northern flank of a regional anticline known as the Swaershoek anticline. The Rooiberg Group records folding and thrusting, which resulted in extensive movement and dismemberment of the Union Tin Member.

The Union Tin Member is characterised by a basal volcaniclastic unit of variable thickness referred to as an ignimbrite by Menge (1963) and as an agglomerate on early geological maps. It consists of isolated angular fragments predominantly of pumice embedded in a fine-grained groundmass composed mainly of interlocking quartz, feldspar and alteration minerals (e.g., Fe-oxide and tourmaline). The fragments vary in size, barely exceeding 5 cm in length, and are variably replaced by chlorite, sericite and Fe-oxide. The ignimbrite unit is overlain by an up to 150 m-thick shale unit, which is characterised by considerable variability in strike and dip as expected from the heavily fractured and dismembered nature of the Union Tin Member. The dominant shale is interbedded with slightly coarser-grained siliceous shale, considered as tuff on early geological maps, and subordinate siltstone and sandstone beds (Menge, 1963). The shale unit is composed chiefly of quartz, sericite, chlorite and Fe-oxides. Generally, the Union Tin Member displays comparable characteristics throughout the Bushveld LIP (Schweitzer et al., 1995).

The structurally-controlled Sn mineralisation in the Union Sn field, as described in detail by Menge (1963), is associated with zones of intense fracturing surrounded by a halo of chlorite-sericite alteration largely in the siliceous shale unit, and occasionally in the underlying ignimbrite unit, of the Union Tin Member. Intense fracturing is attributed to the regional anticlinal folding (Strauss, 1954). Cassiterite is fine-grained (usually ≤100 μm in size) and is commonly intergrown with euhedral magnetite, sericite, chlorite and, occasionally, arsenopyrite, galena, sphalerite, bornite and chalcopyrite. The Sn mineralisation in the Union Sn field resulted from interactions between Sn-bearing fluids and the siliceous shale unit, which is, in comparison to the ignimbrite

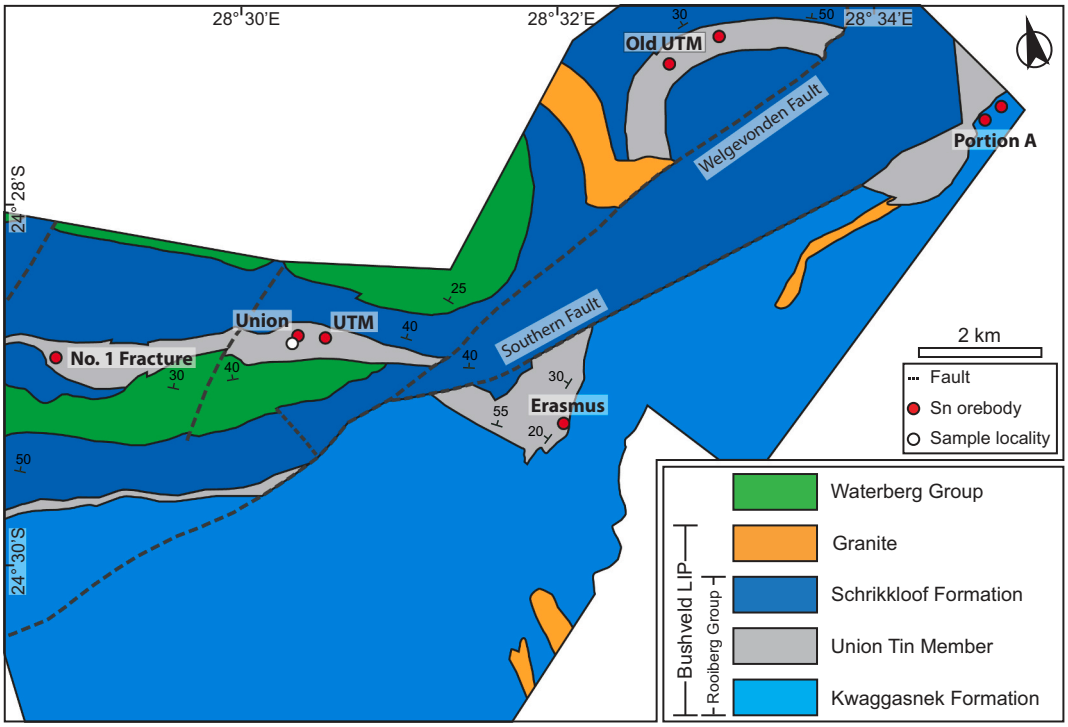

Fig. 3. Geological map of the Union Sn field surrounding the Union Sn mine (modified after Menge, 1963).

unit, more susceptible to folding and fracturing, the latter acting as conduits for ore-bearing fluids likely derived from the Bushveld granites (Strauss, 1954; Menge, 1963). Moreover, the fine-grained nature of the Sn mineralisation probably reflects the fine grain size of the siliceous shale unit, which was variably replaced by the ore mineral assemblage (Strauss, 1954; Menge, 1963).

3.3. Rooiberg Sn field

The Rooiberg Sn field is located within the Rooiberg Fragment that is a relic of the Transvaal Supergroup dominated by the sedimentary rocks of the Pretoria Group, the latter representing the upper part of the Transvaal Supergroup (Fig. 4a–b). Most granitic outcrops are grey-coloured, coarse-grained and unaltered corresponding to the Nebo granite, although highly-altered exposures, locally referred to as the Kenkelbos granite have also been reported from east of the Rooiberg Fragment (Rozendaal et al., 1995). Strauss (1947) equated the Kenkelbos granite with the highly-altered and mineralised Bobbejaankop granite from the Zaaiplaats Sn field. In the Rooiberg Sn field, Sn mineralisation occurs as numerous deposits and prospects all hosted within the Pretoria Group.

The Pretoria Group in the Rooiberg Fragment is, in ascending stratigraphic order, divided into a basal ~1700 m-thick Leeuwpoort Formation (subdivided into a lower Boschoffsberg Quartzite and an upper Blaauwbank Shale) that is conformably overlain by the ~300 m-thick Smelterskop Formation. The Boschoffsberg Quartzite consists mainly of

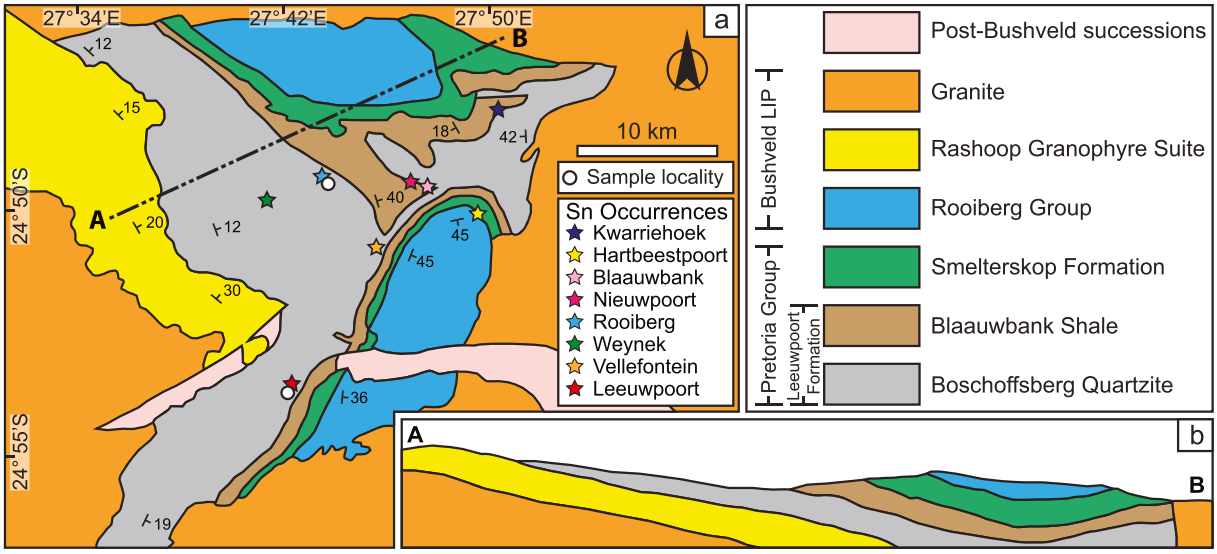

Fig. 4. (a) Geological map of the Rooiberg Sn field; (b) A schematic cross-section (A–B) showing relationships between various rock units (modified after Rozendaal et al., 1995).

cross-bedded feldspathic sandstones displaying an upwardly fining grain size. The Blaauwbank Shale is identified by a lower unit, locally known as the Shaly Quartzite, consisting of a fine-grained sequence of feldspathic quartzite and sandstone with minor interlayers of siltstone with structures typical of a shallow-water environment, and an upper unit, locally referred to as the Main Shale, comprising interlayers of fine-grained laminated sandstone, siltstone and mudstone. The overlying Smelterskop Formation is dominated by thinly-laminated shale horizons with interbedded lenticular feldspathic quartzite, andesitic lavas and locally-developed conglomerates and ignimbrite (Leube and Stumpfl, 1963; Rozendaal et al., 1995).

The Sn mineralisation occurs in two major styles: (1) pocket-type mineralisation is the most common and economically viable style of ore formation involving bedding plane-controlled, cassiterite-bearing miarolitic cavities. These cavities represent partial to complete replacement of the Shaly Quartzite and are associated with faults and fractures typically oriented parallel to the bedding of the sedimentary horizons with a limited lateral extension. The ore mineral assemblage is dominated by cassiterite, tourmaline, carbonates, sericite, pyrite and chalcopyrite. (2) Bedded mineralisation is characterised by thin mineralised veins, occasionally forming stockworks and hydrothermal breccias, laterally extensive that developed sub-parallel to the sedimentary bedding. Minerals associated with the cassiterite ore include disseminations of tourmaline, pyrite, chalcopyrite, sphalerite, carbonates (mainly siderite and ankerite), sericite and minor alkali feldspar and chlorite (Leube and Stumpfl, 1963). These two styles of Sn mineralisation are well-represented by the Rooiberg orebody (or "A-Mine") and the Leeuwpoort orebody (or "C-Mine"), respectively. Despite distribution within a large area, nearly all of the Sn mineralisation in the Rooiberg Fragment occurs along a similar stratigraphic position between the underlying Boschoffsberg Quartzite and overlying Blaauwbank Shale members of the basal Leeuwpoort Formation, which initially prompted a model involving a laterally continuous stratabound Sn horizon (Boardman, 1946). However, further studies indicated a localised, rather than continuous, structurally-controlled zone of Sn mineralisation limited mainly to a horizon immediately below an impermeable

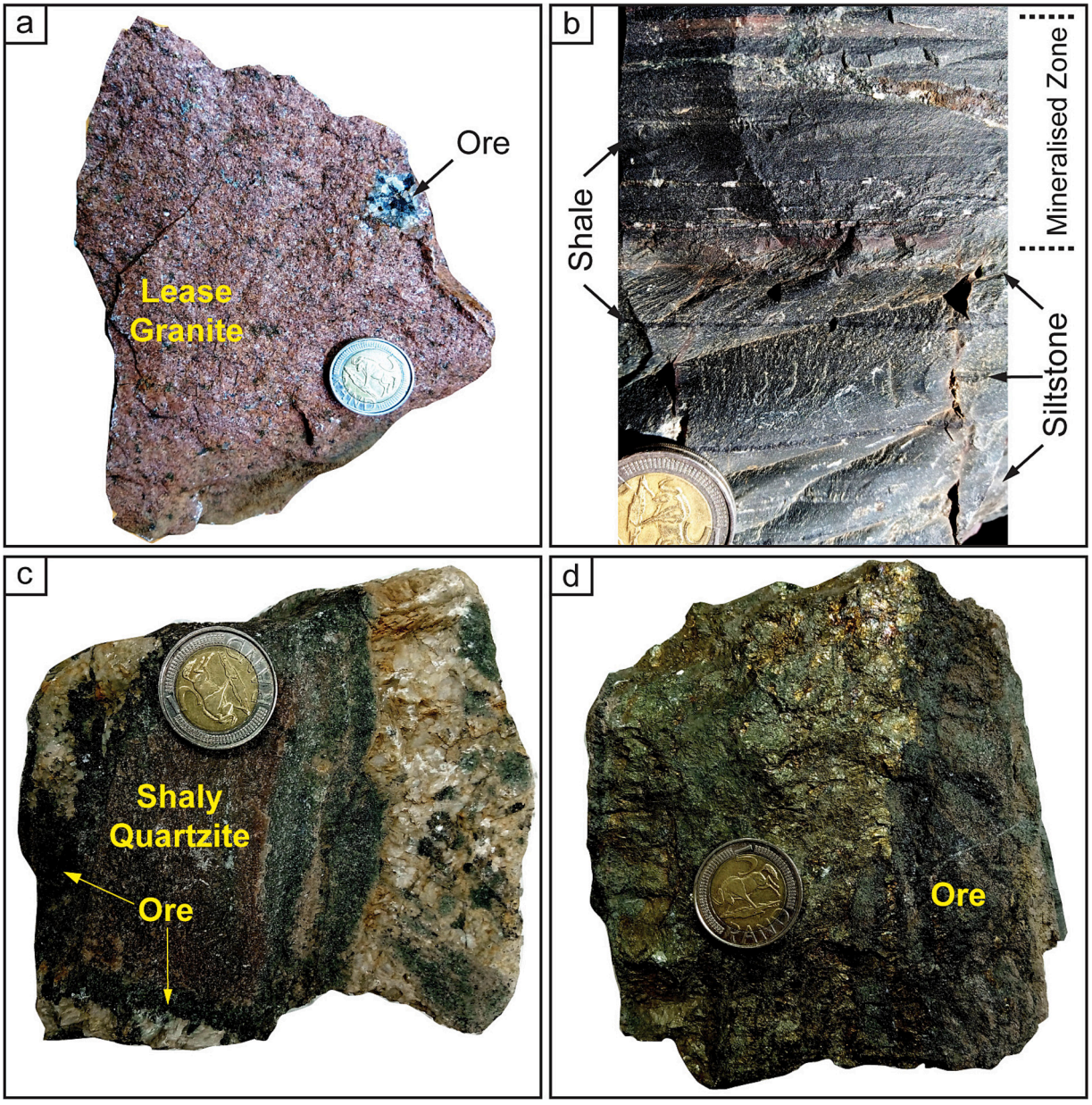

Fig. 5. Photographs of the ore-bearing samples from the Zaaiplaats (a), Union (b) and Rooiberg (c–d) Sn fields. Note that cassiterite from the Union Sn field is fine-grained and difficult to detect in hand specimen.

shale member, which hindered further ascent of the ore-bearing fluid, the latter is tentatively correlated with the Bushveld LIP (Hunter, 1975). A temporal linkage with the Bushveld LIP is also indicated from ages of 2062 ± 9 Ma and 2057 ± 18 Ma reported for two cassiterite samples from the Rooiberg Sn field (Neymark et al., 2018).

4. Sampling and analytical methods

For this study, a number of representative cassiterite-bearing samples were collected from the Zaaiplaats, Union and Rooiberg Sn fields. One sample (sample ZA8) collected from the main ore zone of the Zaaiplaats Sn field includes a highly-altered, fine-grained Lease granite containing miarolitic cavities filled with a hydrothermal mineral assemblage dominated by cassiterite and, to a lesser extent, quartz, alkali feldspar and tourmaline (Fig. 5a). This sample represents a low-grade lenticular style of Sn mineralisation, which forms the bulk of the ore in the Zaaiplaats Sn field. An ore sample of the Union Sn field (sample UT6) was collected from heavy mineral concentrates stockpiled on the mining site, as access to the underground mine workings is no longer possible. These concentrates were derived from Sn mineralisation hosted within the ore-bearing silicified shale horizons containing cassiterite, quartz and Fe-oxides (Fig. 5b). Two cassiterite-bearing samples from the Rooiberg Sn field were studied. One sample (sample LE3) is from the Rooiberg mine (A-Mine), situated in a fragment of the Shaly Quartzite of the Blaauwbank Shale. The Sn mineralisation is stratabound, and cassiterite is present in association with carbonates, alkali feldspar, quartz and tourmaline (Fig. 5c). Another sample (sample LE4) represents a mineralised hydrothermal breccia from the Leeuwpoort mine (C-Mine), characterised by a mineral assemblage dominated by cassiterite, chalcopyrite, pyrite, galena, sphalerite and tourmaline (Fig. 5d).

The ore-bearing samples from the Zaaiplaats and Rooiberg Sn fields contain cassiterite grains of varying size up to several millimetres across, whereas the sample from the Union Sn field, recovered from the heavy mineral concentrates, comprises fine-grained cassiterite ≤100 μm in size. Cassiterite grains were separated by hand picking under a binocular microscope (typically around 200 grains per sample), mounted in epoxy resin disks and polished until the grains were well exposed. Cathodoluminescence (CL) imaging was carried out at the Spectrum Analytical Facility, University of Johannesburg, using a TESCAN Scanning Electron Microscope and an accelerating voltage of 20 kV. Typical CL images were obtained to identify internal textures and select potential target domains for U—Pb isotopic and trace element analysis by Laser-Ablation Inductively Coupled Plasma Mass-Spectrometry (LA-ICP-MS).

Cassiterite LA-ICP-MS trace element analysis was performed using a RESOlution-SE (Australian Scientific Instruments, Fyshwick) 193 nm argon fluoride (ArF) excimer laser system coupled with a Thermo Fisher iCAP RQ ICP-MS, based at the Spectrum Analytical Facility, University of Johannesburg. Using a 60 μm spot size, a beam energy of 6 mJ and a beam attenuation of 50 %, the cassiterite grains were ablated at a repetition rate of 10 Hz and ablation intensity of 4.5 J/cm^2. Helium was used as a carrier gas to provide efficient aerosol transport to the ICP and minimise aerosol deposition. The NIST612 standard glass was used as the bracketing external standard. Samples were analysed in separate runs comprising 15 analyses of unknowns bracketed before and after by analyses of the NIST610 standard glass and the BCR2G basaltic glass during each run as independent controls on reproducibility and instrument stability. The ^{119}Sn isotope was used as the internal standard, assuming stoichiometric SnO_2 for quantification purposes. Data were processed using the GLITTER software (Van Achterbergh et al., 2001). Only inclusion- and fracture-free regions of the cassiterite grains were targeted, although some tiny inclusions may have been ablated due to the relatively large diameter of the laser beam (60 μm). All signals were filtered for spikes or inclusions.

Based on optical microscopy, backscattered-electron (BSE) and CL imaging, cassiterite domains without obvious mineral inclusion, microcracks and alteration, were selected for LA-ICP-MS U—Pb isotopic analysis at the State Key Laboratory for Mineral Deposits Research, Nanjing University, China. The analysing system comprises a Thermo Fisher iCAP Qc ICP-MS coupled with an ASI RESOlution LR 193-nm ArF laser that uses a large laser ablation cell (155 × 105 mm). About 99 % of the material ablated was washed out in <1.5 s due to the two-volume laser ablation cell. Cassiterite grains were analysed using a laser energy density of 4 J/cm^2, spot sizes of 74 and 43 μm and a repetition rate of 6 Hz. Four U—Pb reference and validation materials were used including the Cligga Head (CLGH) cassiterite from Cornwall, southwest England (TIMS U—Pb age = 285.14 ± 0.25 Ma; Tapster and Bright, 2020), the Yankee (YK) cassiterite from a lode related to the Mole granite, New England Orogen, Australia (TIMS U—Pb age = 246.48 ± 0.51 Ma; Carr et al., 2020), the Jian-1 cassiterite from a quartz-wolframite deposit, Chongyi county, Southern Jiangxi Province, China (TIMS U—Pb age = 154.969 ± 0.041 Ma; Tapster and Bright, 2020) and the XHL cassiterite from Xianghualing skarn Sn deposit, Southern Hunan Province, China (~152–154 Ma). The reference and validation materials were analysed twice with every 12 and 6 unknown sample analyses, respectively. Each spot analysis incorporated a background acquisition of approximately 20 s, followed by 40 s of sample data acquisition. Isotope compositions were measured in a time resolved mode. For U—Pb analysis, dwell times for each mass scan were 8 ms for ^{204}Pb, 15 ms for ^{206}Pb and ^{208}Pb, 20 ms for ^{238}U, ^{232}Th and ^{207}Pb. Raw data reduction was performed offline using Iolite software (ver. 4). The analytical and data reduction procedures are described in Zhang et al. (2017a, 2017b). Isoplot (ver. 4.15) was employed to calculate Tera-Wasserburg ^{207}Pb/^{206}Pb versus ^{238}U/^{206}Pb (U—Pb) and ^{207}Pb/^{206}Pb versus ^{208}Pb/^{206}Pb Pb—Pb isochron ages following the procedure recommended for cassiterite dating outlined in Neymark et al. (2018).

5. Results

5.1. Cassiterite morphology and texture

Representative CL images of analysed cassiterite samples from the Zaaiplaats, Union and Rooiberg Sn fields are presented in Fig. 6. The cassiterite grains separated from the Zaaiplaats Sn field are large (averaging 500 μm in size) and anhedral to euhedral, and show a faint micrometre-scale oscillatory zoning dominated by dark zones with thin interlayers of bright zones (Fig. 6a). The mm-sized cassiterite grains of the Rooiberg Sn field are subhedral to euhedral and, unlike those of the Zaaiplaats Sn field, show a well-defined micrometre-scale oscillatory zoning (Fig. 6b). In contrast, the fine-grained ≤100 μm in size cassiterite grains from the Union Sn field are usually cracked and inclusion-rich, and intergrown with sericite, quartz and magnetite, thus showing irregular and relatively complex zoning patterns (Fig. 6c). A limited number of cassiterite grains from the Union Sn field that are not intergrown with other minerals, display an oscillatory zoning comparable to that reported for the Rooiberg Sn field.

5.2. Cassiterite trace element compositions

In total, 182 cassiterite grains were analysed from the Zaaiplaats (n = 54), Rooiberg (n = 109) and Union (n = 19) Sn fields. The entire dataset of the LA-ICP-MS derived trace element abundances is presented in Appendix A. Inter-element relationships between various trace elements and chondrite-normalised REE patterns are displayed in Figs. 7 and 8, respectively.

The most abundant elements in the cassiterite samples are Fe (170 to 16,500 ppm), W (1 to 32,000 ppm) and Ti (1 to 17,000 ppm). The cassiterite samples from the Zaaiplaats Sn field are comparatively depleted in these elements, whereas, although highly variable, those of the Union Sn field show higher abundances of Fe and Ti, while those of the Rooiberg Sn field are characterised by higher W contents. The

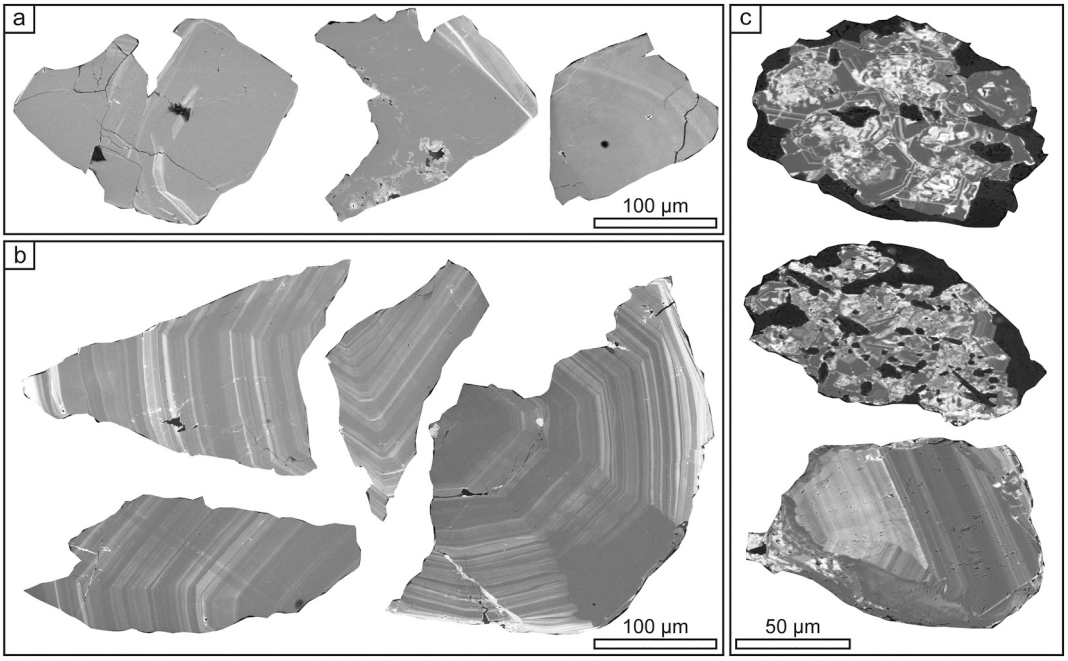

Fig. 6. Representative CL images of cassiterite from the Zaaiplaats (a), Rooiberg (b) and Union (c) Sn fields. Note that most cassiterite grains from the Union Sn field are intergrown with magnetite, sericite and quartz.

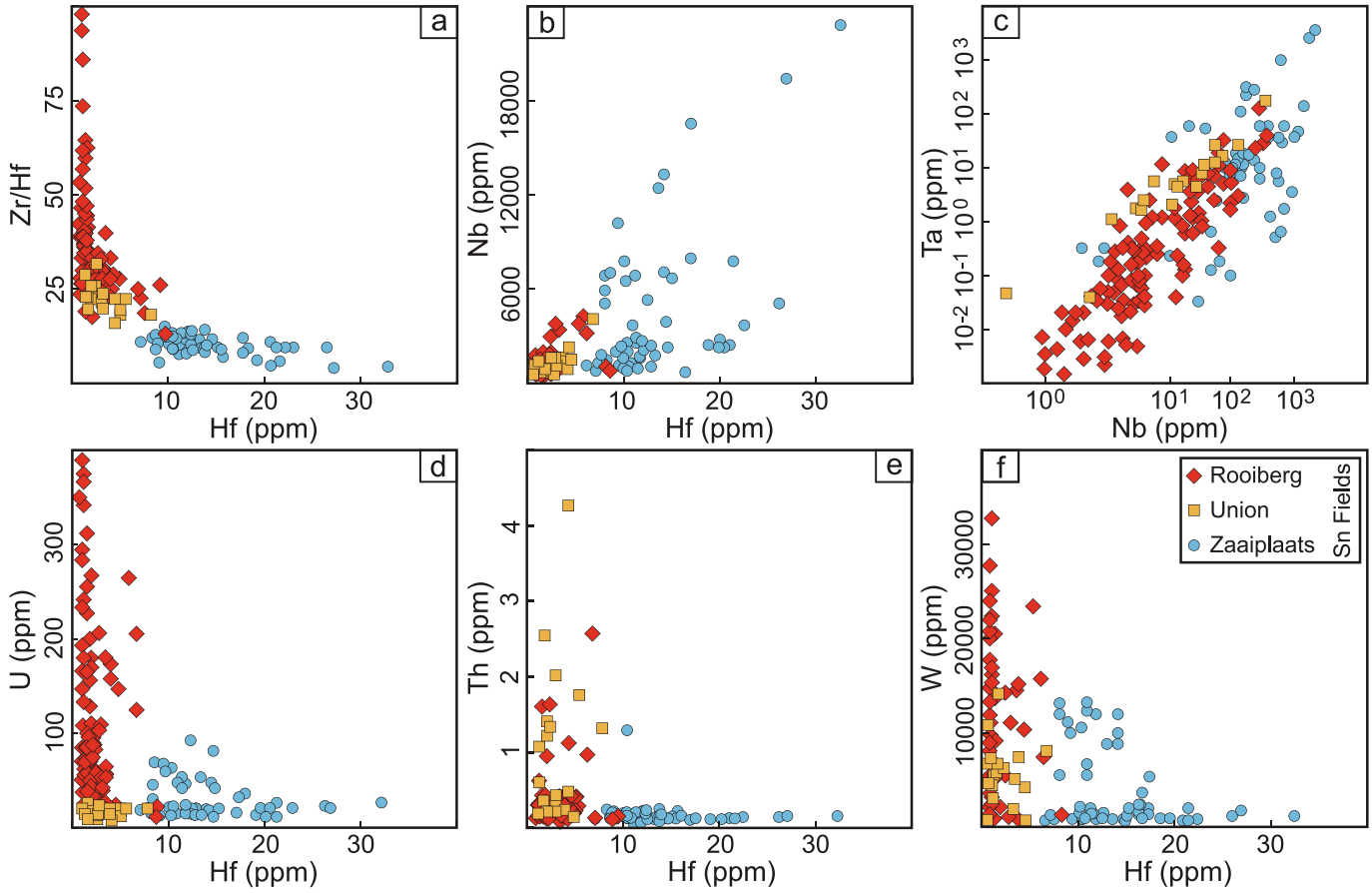

Fig. 7. Variation diagrams for a selection of trace elements in cassiterites from the Zaaiplaats, Union and Rooiberg Sn fields.

cassiterite grains from the Rooiberg (mean Zr = 50 ppm; mean Hf = 2.5 ppm) and Union (mean Zr = 55 ppm; mean Hf = 2.2 ppm) Sn fields are defined by lower Zr and Hf values than those from the Zaaiplaats Sn field (mean Zr = 180 ppm; mean Hf = 14 ppm). The cassiterite samples from the Rooiberg (Zr/Hf = 20–105) and Union (Zr/Hf = 20–40) Sn fields exhibit more variable Zr/Hf ratios than those of the Zaaiplaats Sn field

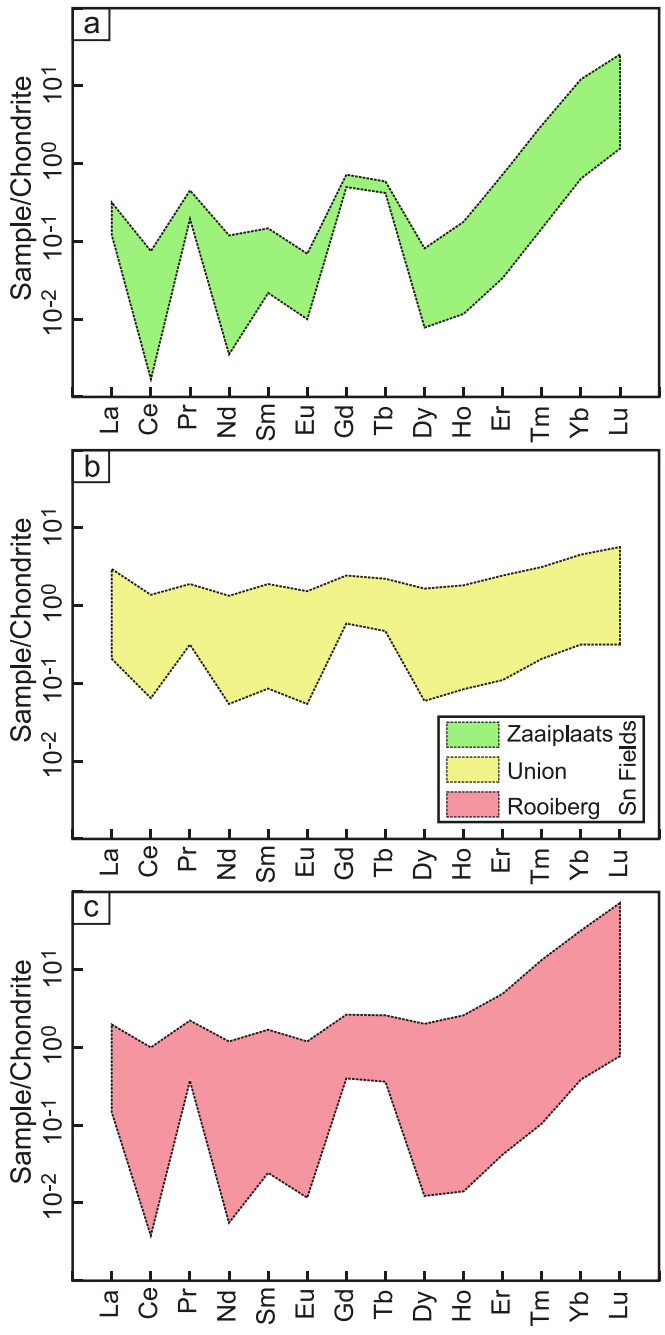

Fig. 8. Chondrite-normalised REE plots of cassiterite analyses from the Zaaiplaats (a), Union (b) and Rooiberg (c) Sn fields. Chondrite normalising values are from Taylor and McLennan (1985).

(Zr/Hf = 7–20) (Fig. 7a). Other high-field strength elements (HFSE) including Nb and Ta appear in detectable quantities in all of the cassiterite grains. The Zaaiplaats Sn field is identified by cassiterite that is markedly enriched in Nb (averaging 4160 ppm) and Ta (averaging 215 ppm), compared to those from the Rooiberg (mean Ta = 1.5 ppm; mean Nb = 80 ppm) and Union (mean Ta = 17 ppm; mean Nb = 470 ppm) Sn fields (Fig. 7b–c). The cassiterite samples from the Rooiberg Sn field (mean U = 60 ppm; Th = <3 ppm) have the highest U values, whereas Th content remains very low in all the Sn fields (Zaaiplaats: mean U = 22 ppm; Th = <2 ppm and Union: mean U = 7 ppm; Th = <4 ppm) (Fig. 7d–e). Moreover, as described above, the Rooiberg and Union Sn fields show enrichments in W relative to the Zaaiplaats Sn field (Fig. 7f). In summary, Fig. 7 indicates that cassiterites from the endogranitic Zaaiplaats Sn field are enriched in a variety of metals particularly HFSE such as Zr, Hf, Nb and Ta compared to those from the Rooiberg and Union Sn fields, suggesting that the endogranitic fluid from which the Zaaiplaats cassiterites precipitated was more enriched in those elements than those forming from more distal fluids.

The chondrite-normalised REE patterns of all the cassiterite grains are comparable and characterised by quasi-parallel patterns as indicated by the relatively restricted variations of $La_N/Sm_N = \leq 10$ and $Gd_N/Yb_N = \leq 3$ (Fig. 8). The patterns are characterised by an overall enrichment in the heavy (H) REE compared to the light (L) REE (Fig. 8). The total REE abundance (ΣREE = <16 ppm) is low, with restricted variability and range in the Zaaiplaats cassiterite grains (mean ΣREE = 2 ppm), but higher abundances and greater variability in those from Union (mean ΣREE = 5 ppm) and Rooiberg (mean ΣREE = 5 ppm). Notably, the cassiterite grains from the Union Sn field are more enriched in LREE (mean La/Yb = 2.2; mean LREE = 3 ppm; mean HREE = 1.2 ppm), whereas those of the Rooiberg Sn field have higher HREE values (mean La/Yb = 0.3; mean LREE = 1.1 ppm; mean HREE = 3.6 ppm). In all cases, the cassiterite samples are defined by a restricted range of LREE, varying by only one order of magnitude, whereas HREE show a much greater variation, differing by more than two orders of magnitude. All of the cassiterite grains display variable Ce anomalies (Ce/Ce*), although those from the Zaaiplaats Sn field show a wider variation (Ce/Ce* = 1–4.2), compared to those from Rooiberg (Ce/Ce* = 0.7–1.7) and Union (Ce/Ce* = 0.7–1) Sn fields. In contrast, although all the cassiterite samples exhibit negative Eu anomalies (Eu/Eu*), those from the exogranitic Union (Eu/Eu* = 0.3–2.1) and Rooiberg (Eu/Eu* = 0.06–0.6) fields show a broader variation compared to the endogranitic Zaaiplaats field (Eu/Eu* = 0.05–0.3).

5.3. *Cassiterite geochronology*

Four samples were selected for U—Pb dating, including one sample from Zaaiplaats, two samples from Rooiberg and one sample from Union (Fig. 5). The Pb—Pb isochron ages were calculated for cassiterite samples from Zaaiplaats Sn field (sample ZA8), and Rooiberg Sn field (samples LE3 and LE4). However, a concordia-intercept age on a Tera-Wasserburg diagram was preferred for sample UT6 from the Union Sn field because of its higher Th abundances. The U—Pb and Pb—Pb isochrons, calculated ages, and isotope data for the cassiterite samples are provided in Fig. 9 and Appendix B. Collectively, a total of 139 analyses (nine analyses were excluded from age calculations) were conducted on cassiterite grains apparently free of inclusions or fractures, although tiny inclusions could not be avoided during analysis. The fine-grained nature of the cassiterite ore from the Union Sn field permitted only a limited number of analysis.

Thirty-three analyses of sample ZA8 from the Zaaiplaats Sn field produced a Pb—Pb isochron age of 2061 ± 9 Ma (Fig. 9a). Forty analyses of sample LE3 from the Rooiberg mine (A-Mine) and 34 analyses of sample LE4 from the Leeuwpoort mine (C-Mine) of the Rooiberg Sn field yielded Pb—Pb isochron ages of 2054 ± 3 Ma (Fig. 9b) and 2059 ± 5 Ma (Fig. 9c), respectively. Moreover, 23 analyses of sample UT6 from the Union Sn field, with $Th/^{206}Pb$ ratios of >0.01, returned a Tera-Wasserburg lower intercept U—Pb age of 2061 ± 40 Ma (Fig. 9d).

6. Discussion

6.1. *Timing of Sn mineralisation*

The cassiterite ages from the four studied samples are comparable and, within the precision of the method used, fall within a relatively restricted range from 2061 ± 40 Ma to 2054 ± 3 Ma. These ages are regarded as statistically indistinguishable and, consequently, the ages returned from the Bushveld Sn fields appear to record a single Sn mineralisation event associated with the Bushveld LIP. Available geochronological data from the Bushveld LIP and spatially associated *syn-*

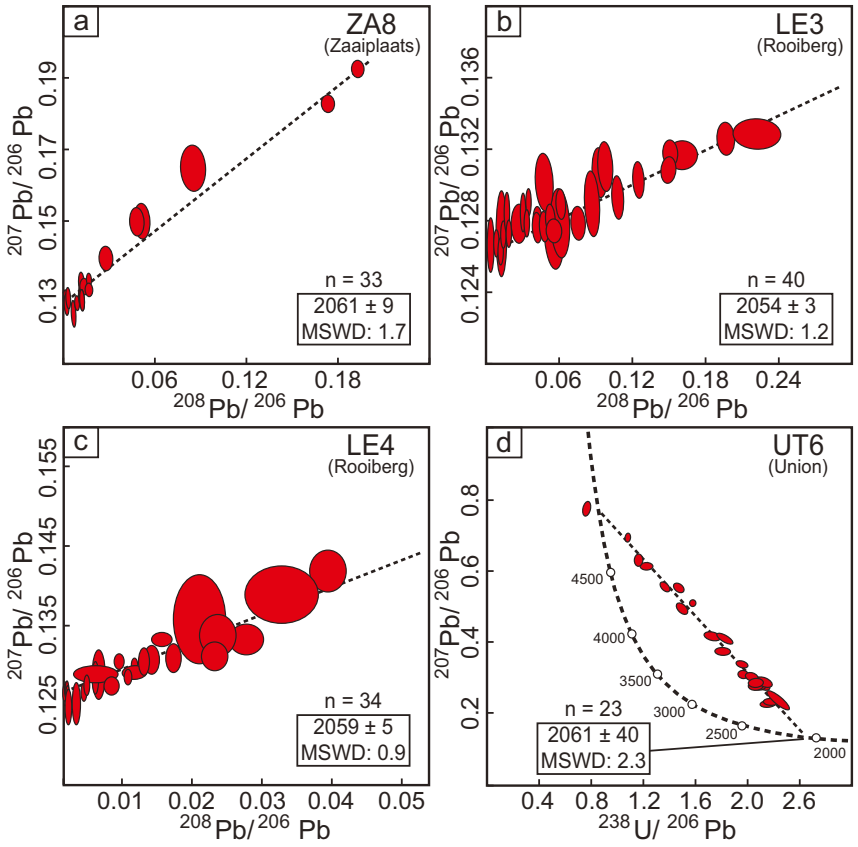

Fig. 9. $^{207}Pb/^{206}Pb$ versus $^{208}Pb/^{206}Pb$ Pb—Pb isochron ages for cassiterite samples from Zaaiplaats (a) and Rooiberg (b–c) Sn fields and (d) Tera-Wasserburg concordia diagram for cassiterites from the Union Sn field. MSWD: Mean square of weighted deviates.

Bushveld intrusions suggest a three-stage (2061–2060 Ma, 2059–2054 Ma and 2046–2042 Ma, Scoates et al., 2021 and references therein) emplacement mechanism for the Bushveld LIP. The earliest stage (2061–2060 Ma) is represented by the volcanic Rooiberg Group (2061 ± 2 Ma; Walraven, 1997) which shares an age with the nearby Phalaborwa Complex (2060 ± 0.5 Ma; Wu et al., 2011). The second and main stage is recorded by the 2059–2054 Ma rocks reported from the RLS, RGS and LGS (Scoates et al., 2021), although high-precision dating of the RLS demonstrates a short-lived emplacement and crystallisation over an interval of one million years (2057.7 ± 1.6 Ma, Olsson et al., 2010; 2055.9 ± 0.2 Ma to 2054.8 ± 3 Ma, Zeh et al., 2015). This short time interval overlaps with the emplacement of a number of adjacent igneous complexes such as the Marble Hall Complex (2055 ± 3 Ma; De Waal and Armstrong, 2000), the Lindeques Drift Complex (2054 ± 5 Ma; De Waal et al., 2006) and the Uitkomst Complex (2057 ± 0.6 Ma; Maier et al., 2018). The third stage (2046–2042 Ma) is recorded specifically by the Thabazimbi sills (2046.6 ± 3.4 Ma; Rajesh et al., 2013). A well-received hypothesis in relation to the origin of the Bushveld LIP and temporally associated igneous complexes, suggests that the arrival of a plume sourced from the asthenosphere (Rajesh et al., 2013) or from the deep mantle (Zirakparvar et al., 2019) into the base of the continental lithosphere resulted in an extensive partial melting of the lithospheric mantle beneath the Kaapvaal Craton leading to the emplacement of basaltic and rhyolitic lavas (Rooiberg Group) and carbonatite magmas (e.g., Phalaborwa Complex). Generally, carbonatite magmas are characterised by a preference for low degrees of partial melting representing the earliest stage in the evolution history of a LIP (Rajesh et al., 2013 and references therein). Moreover, this hypothesis proposes that subsequent pulses of magmatism, within a few million years of the initial stage of magmatism, are a result of the reactivation of the original plume.

The age range yielded by the cassiterite samples from the Zaaiplaats, Union and Rooiberg Sn fields (2061 ± 40 Ma to 2054 ± 3 Ma, Fig. 9) compares well with the main stage of the emplacement of the Bushveld LIP (2059–2054 Ma, Scoates et al., 2021), during which most mafic-ultramafic and granitic-granophyric rocks of the RLS, RGS and LGS were emplaced. Notably, cassiterite remained unaffected by significant magmatic and hydrothermal activity subsequent to the emplacement of the Bushveld LIP (e.g., McNaughton et al., 1993). The age range of 2061 ± 40 Ma to 2054 ± 3 Ma returned from the cassiterite samples of the Bushveld LIP is much younger than an age of 2099 ± 3 Ma previously reported for cassiterites from the Zaaiplaats Sn field (Gulson and Jones, 1992), but is comparable with the ages of 2062 ± 9 Ma and 2057 ± 18 Ma documented for cassiterites from the Rooiberg Sn field (Neymark et al., 2018).

The cassiterite analyses from the Union Sn field have generated a relatively poorly-constrained age of 2061 ± 40 Ma, consistent with the fractured and porous nature of these grains. The Union Sn field is spatially associated with the Welgevonden Fault (Fig. 3), which is a prominent component of the Thabazimbi-Murchison Lineament that forms the southern boundary of the northern limb of the Bushveld LIP. This fault hosts the vein-type Waterberg platinum deposit, which formed by the leaching of ore metals from mafic rocks of the Bushveld LIP (McDonald et al., 1995). Thus, the dissolution-precipitation textures associated with the cassiterite grains from the Union Sn field may have been induced by post-Bushveld hydrothermal fluids, which resulted in variably discordant cassiterite ages (Fig. 9d).

6.2. *Substitution mechanisms in cassiterite*

A large number of trace elements are observed to have substituted into the Bushveld cassiterites. These trace elements can be used to determine processes involved in the Sn mineralisation and composition

of the source magmas or fluids (Cheng et al., 2019; Gemmrich et al., 2021; Liu et al., 2021). The cassiterite samples associated with the Bushveld LIP are distinguished by highly variable trace element contents (Figs. 7–8). Excessive or non-systematic elemental enrichments result mainly from a combination of complex substitutions of trace elements into the cassiterite structure, as well as the presence of tiny inclusions (Möller et al., 1988).

Cassiterite has a tetragonal structure with Sn^{4+} in sixfold coordination and, hence, the following elements are compatible with respect to cassiterite and can potentially be accommodated into its crystal lattice: Mn^{2+}, Fe^{2+}, Ti^{3+}, Al^{3+}, In^{3+}, Fe^{3+}, Ga^{3+}, Cr^{3+}, Sc^{3+}, Sb^{3+}, REE^{3+}, W^{4+}, U^{4+}, Th^{4+}, Zr^{4+}, Hf^{4+}, Ti^{4+}, V^{5+}, Nb^{5+} and Ta^{5+} (Murciego et al., 1997). These elements appear in appreciable quantities in the studied cassiterites, although there are significant compositional differences between various Sn fields. The tetravalent cations (Zr^{4+}, Hf^{4+}, Ti^{4+}, U^{4+}, W^{4+}) share a similar charge and ionic radii with, and are able to directly substitute for, Sn^{4+}, without the necessity for any specific charge-balanced substitution mechanism (e.g., $Zr^{4+} \leftrightarrow Sn^{4+}$). Cations with an ionic charge other than 4+, however, require charge-balanced coupled substitution mechanisms.

Niobium and Ta have similar ionic charge and ionic radii, and hence display comparable geochemical behaviour (Fig. 7c). However, a large variation in the concentration of Nb^{5+} and Ta^{5+} is commonly reported from cassiterite analyses worldwide, which is usually attributed to various mechanisms including fractionation during mineral growth and interaction with hydrothermal fluids (Lerouge et al., 2017). A coupled substitution by a combination of 3+ and 5+ cations for two Sn^{4+} ions is likely the most common substitution mechanism in cassiterite [e.g., $(Nb, Ta)^{5+} + Fe^{3+} \leftrightarrow 2Sn^{4+}$] (Möller et al., 1988; Murciego et al., 1997). Such a substitution mechanism is responsible for the incorporation of the bulk of the trivalent cations (Fe^{3+}, In^{3+}, Al^{3+}, Ga^{3+}, Cr^{3+}, Sc^{3+}, Sb^{3+}) as well as 5+ cations (V^{5+}, Nb^{5+}, Ta^{5+}) into the cassiterite structure. A positive correlation between Sc and V (Fig. 10a), for example, suggests that V substitutes in the 5+ state, and because Sc appears as only one valence (3+) state under most geological conditions, a likely substitution mechanism is $V^{5+} + Sc^{3+} \leftrightarrow 2Sn^{4+}$. As shown in Fig. 10b, Σ3+ cations show no linear correlation with Σ5+ cations, and most 3+ cations lie above the 1:1 ratio line, indicating that an additional mechanism

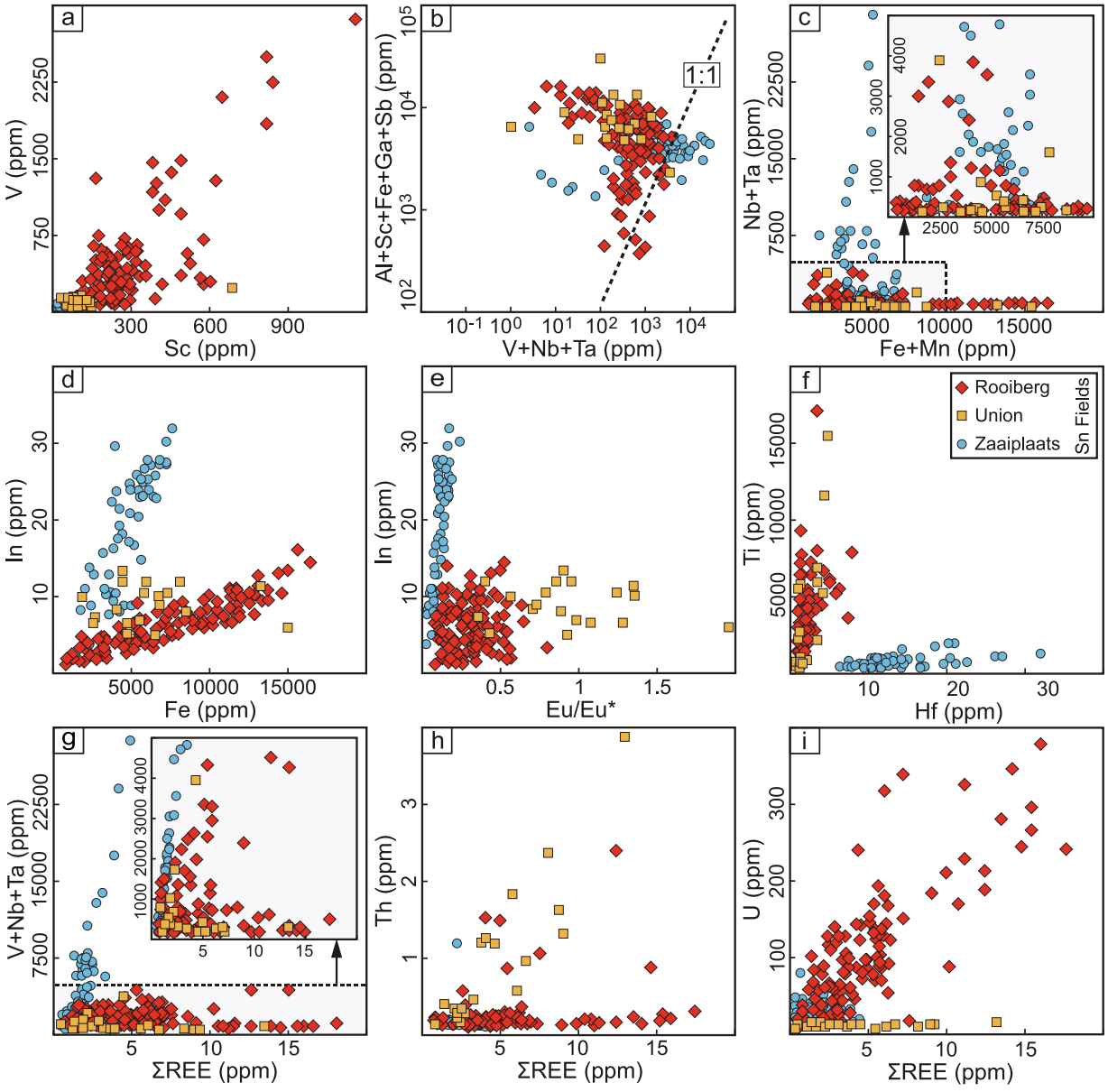

Fig. 10. Variation diagrams of a selection of trace elements and Europium anomaly ($Eu/Eu^* = Eu_{cn}/[Sm_{cn} \times Gd_{cn}]^{0.5}$) for cassiterite samples from the Zaaiplaats, Union and Rooiberg Sn fields.

contributed to the incorporation of 3+ cations into the cassiterite structure. A potential substitution mechanism is 3+ cation + $H^+ \leftrightarrow Sn^{4+}$, as previously suggested for cassiterite samples elsewhere (Möller et al., 1988).

The 2+ cations are incorporated into the cassiterite lattice in association with the 5+ cations through a charge-balanced coupled substitution mechanism involving $2(Nb, Ta)^{5+} + (Fe, Mn)^{2+} \leftrightarrow 3Sn^{4+}$, representing an isomorphous solid solution between cassiterite and the tapiolite group [$(Fe, Mn)(Ta, Nb)_2O_6$], the latter having a similar tetragonal structure to cassiterite (Tindle and Breaks, 1998). This substitution mechanism is significant particularly in cassiterites from the Zaaiplaats Sn field, and is characterised by a near linear correlation between Mn + Fe and Nb + Ta (Fig. 10c), suggesting that the Zaaiplaats cassiterites contain Fe in a divalent state. Iron appears in two valences including Fe^{3+} and Fe^{2+}, both of which can occur together in cassiterite, although Fe^{3+} more readily substitutes for Sn^{4+} due to the smaller charge difference (Lerouge et al., 2017). Incorporation of various valences of Fe depends strongly on the oxidation state and temperature of the ore-forming melt. An oxidising environment is reflected by the relative abundance of Fe^{3+}, whereas a reducing environment and/or high temperature (≥300 °C) preferentially stabilises Fe^{2+} (Murciego et al., 1997). Excess of Fe^{3+} can be charge compensated by the presence of OH^- in the cassiterite structure ($Fe^{3+} + OH^- \leftrightarrow Sn^{4+} + O^{2-}$) (Losos and Beran, 2004).

Notably, the cassiterite samples from the Zaaiplaats Sn field display a positive correlation between In and Fe (Fig. 10d), and are characterised by a relative enrichment of In (mean = ~20 ppm), compared to those from the Union (mean = ~8 ppm) and Rooiberg (mean = ~5 ppm) Sn fields. Indium only appears in a trivalent state, which, similar to other 3+ cations associated with 5+ cations described above, can substitute for Sn^{4+}. However, the positive correlation between In and Fe requires a substitution mechanism for these two elements. The cassiterite samples demonstrate distinct trends, namely a high-In/low-Fe trend represented by the Zaaiplaats Sn field and a low-In/high-Fe trend characterised by the Rooiberg and Union Sn fields (Fig. 10d). Such distinct trends are interpreted to represent the preferred incorporation of different oxidation states of Fe, with the high-In trend corresponding to the dominance of a substitution mechanism involving Fe^{2+} ($2In^{3+} + Fe^{2+} \leftrightarrow 2Sn^{4+}$), and the low-In trend consistent with the predominance of Fe^{3+} through an $(In, Fe)^{3+} + (Nb, Ta)^{5+} \leftrightarrow 2Sn^{4+}$ substitution mechanism (Lerouge et al., 2017). Similarly, the cassiterite analyses reveal correlations between In and Eu/Eu*, the latter representing a prominent redox-sensitive indicator, which also exhibit two distinct trends. These are a high-In/low-Eu/Eu* trend represented by the Zaaiplaats Sn field and a low-In/high-Eu/Eu* trend displayed by the Rooiberg and Union Sn fields (Fig. 10e). Moreover, the cassiterite samples display two distinct trends with respect to Ti and Hf including a high-Ti/low-Hf trend with a well-developed positive correlation between Ti and Hf represented by the Rooiberg and Union Sn fields and a low-Ti/high-Hf trend with a poorly-defined correlation between Ti and Hf defined by the Zaaiplaats Sn field. The high-Ti/low-Hf trend potentially arises from the incorporation of Ti^{4+} into the cassiterites from the Union and Rooiberg Sn fields, hence developing a positive association with Hf^{4+} (and Sn^{4+}), while the low-Ti/high-Hf trend shows the dominance of Ti^{3+} in cassiterites of the Zaaiplaats Sn field (Fig. 10f). These findings are in agreement with the above-described observations that Fe, like Mn^{2+}, occurs mainly in a divalent state in the Zaaiplaats cassiterites. By contrast, the cassiterite samples from the Rooiberg and Union Sn fields preferentially incorporated Fe^{3+}. Generally, the distribution of the multivalent elements appears to indicate a more reducing environment of formation for the cassiterites of the Zaaiplaats Sn field relative to those of the Rooiberg and Union Sn fields.

Similar to other 3+ cations, REE^{3+} are incorporated into the cassiterite structure together with 5+ cations [$(Nb, Ta, V)^{5+} + REE^{3+} \leftrightarrow 2Sn^{4+}$]. This mechanism is responsible for the incorporation of the entire REE budget into the cassiterites of the Zaaiplaats Sn field, as inferred by a nearly co-linear positive correlation between ΣREE and V + Nb + Ta (Fig. 10g). Such a substitution mechanism also partly accounts for the incorporation of REE into the cassiterite samples from the Union and Rooiberg Sn fields. However, most cassiterite analyses from these two Sn fields show elevated REE with no particular relationship with V + Nb + Ta, suggesting that the presence of REE in these cassiterites is attributable to a different mechanism. The observations that the cassiterites from the Union and Rooiberg Sn fields display REE that are broadly positively correlated with Th (Fig. 10h) and U (Fig. 10i), raise the potential for the presence of tiny phosphates that usually host significant quantities of REE such as xenotime [$(Y, HREE)(PO_4)$], apatite, monazite [$(LREE, Th)(PO_4)$] and florencite [$LREEAl_3(PO_4)_2(OH)_6$] (Nazari-Dehkordi et al., 2019). Nonetheless, the cassiterites have remarkably low values of REE (<16 ppm) and Th (<4 ppm) suggesting that the cassiterite samples with low V + Nb + Ta values from the Union and Rooiberg Sn fields may have incorporated REE through a substitution mechanism involving H+ [$Sn^{4+} \leftrightarrow REE^{3+} + H^+$] (Möller et al., 1988), as discussed above.

Collectively, the trace element compositions of cassiterite samples record the conventional charge-balanced substitution mechanisms documented in cassiterite elsewhere. However, the cassiterites from the Zaaiplaats Sn field are enriched predominantly in Ta, Nb, In, Zr and Hf, and represent a more reducing environment than those of the Union and Rooiberg Sn fields that are characteristically rich in W, Ti, U, Th, Fe and Mn. These differences are further discussed below.

6.3. Implications for Sn metallogeny

Globally, primary tin deposits are associated with granites (Heinrich and Eadington, 1986), and also, to a lesser extent, with volcanogenic massive sulphide (VMS) and sedimentary-exhalative (SEDEX) deposits (e.g., Neves Corvo Cu—Sn VMS deposit, Portugal: Oliveira et al., 1997; Sullivan Fe-Pb-Zn-Sn SEDEX deposit, Canada: Hamilton et al., 1982). Trace element compositions of cassiterite can effectively distinguish between environments of Sn formation (Möller et al., 1988; Murciego et al., 1997; Hennigh and Hutchison, 1999). In particular, cassiterite orebodies associated with granites display higher Fe and W values than those of the SEDEX/VMS family. Enrichment of W and Fe in granite-related cassiterite is due mainly to the highly-fractionated characteristics of the associated granites, whereas a depletion in Fe in cassiterites from SEDEX/VMS deposits arises from the strongly-reduced nature of the ore-bearing fluids which favours Fe^{2+} and precipitates Fe-sulphides rather than Fe-oxides (Hennigh and Hutchison, 1999). The trace element data for cassiterites from the Zaaiplaats, Union and Rooiberg Sn fields show W and Fe values consistent with derivation from a granitic melt (Fig. 11), which agrees with the geological setting of these deposits.

The trace element dataset reveals distinct compositions and varying redox states for the cassiterites from various Sn fields associated with the Bushveld LIP. The cassiterite samples from the Union Sn field develop compositions that are broadly comparable to those of the Rooiberg Sn field. This is likely related to the limited number of analyses available from the Union Sn field.

The compositional differences observed in the endogranitic and exogranitic cassiterites appear to correspond to proximity to the causative granitic intrusion, with the endogranitic Zaaiplaats Sn field representing a proximal Sn field, compared to the exogranitic Rooiberg and Union Sn fields that are more distal in character. The evolved nature of the cassiterite samples from the Zaaiplaats Sn field is well reflected by Zr/Hf ratios. Zirconium and Hf exhibit similar geochemical behaviour and maintain a near-chondritic Zr/Hf ratio, varying in the range of 35–40, in most geological environments (Hoskin and Schaltegger, 2003). Minerals formed under hydrothermal environments and from highly-differentiated igneous rocks, however, usually develop Zr/Hf ratios that are significantly different from chondritic values. Such fractionation may result from various processes including early crystallisation of minerals with the ability to fractionate Zr such as zircon

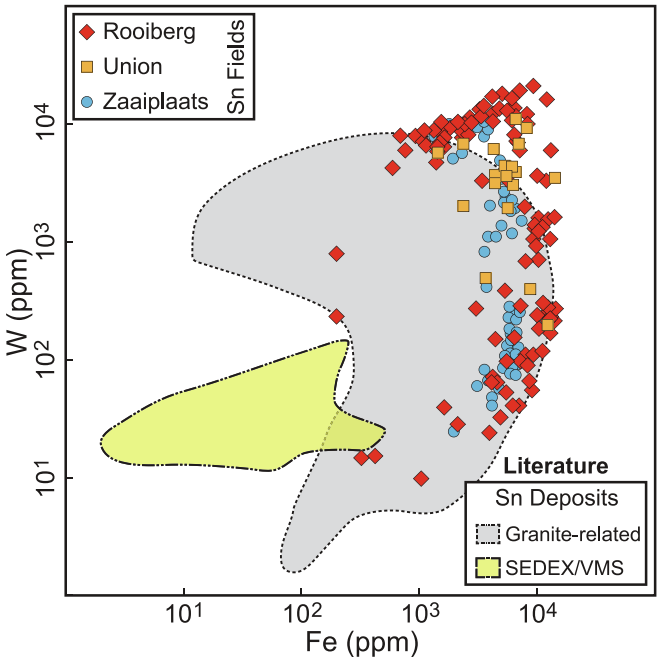

Fig. 11. Discrimination diagram of W (ppm) versus Fe (ppm) showing that all the Sn fields are related to a granitic source. Compositional fields are from Guo et al. (2018). SEDEX: Sedimentary-exhalative; VMS: Volcanogenic massive sulphide.

(Linnen, 1998), hydrothermal alteration (Rubin et al., 1993; Bau, 1996) and preferential mobilisation of Zr into B-F-bearing fluids (Haapala, 1997). Despite a marked variation, the Zr/Hf values of cassiterites systematically decrease from the Rooiberg (Zr/Hf = 20–105) and Union (Zr/Hf = 20–40) to Zaaiplaats (Zr/Hf = 7–20; Fig. 7a). This relates to the high contents of Zr and Hf in the endogranitic cassiterites from the Zaaiplaats Sn field that are usually associated with a melt greatly enriched in F and B (Rubin et al., 1993). Such a melt is also indicated by the presence of F-B-bearing phases such as bastnaesite, synchysite and fluorite within the Zaaiplaats ore mineral assemblage (McNaughton et al., 1993). These F-B-bearing phases have not been reported from the ore mineral assemblages associated with the Rooiberg and Union Sn fields.

A potential explanation for the discrete compositions of the endogranitic and exogranitic cassiterites is that the Union and Rooiberg Sn fields derived from granitic intrusions that were different from that of the granite-hosted Zaaiplaats Sn field. These granitic intrusions formed within a short time interval as indicated by the overlapping ages (Fig. 9), and likely had different compositions and varying redox states, although the comparable REE patterns reported from the Bushveld Sn fields suggest a common origin for all the granitic intrusions.

Another scenario is that the Sn mineralisation is related to a single granitic intrusion and that the distinct compositions are due to an ore-forming mechanism involving fluid boiling whereby an initially homogenous fertile granitic melt is divided into a high-salinity liquid and a co-existing vapour phase with a markedly lower salinity. These liquid and vapour phases have the ability to accommodate significant quantities of trace elements controlled mainly by their complexation behaviour (Shmulovich et al., 2002; Monecke et al., 2011). In other words, elemental depletions or enrichments observed in one phase are usually mirrored in the co-existing phases. The existing literature appears to support the involvement of fluid boiling in the formation of the Bushveld Sn fields. Available fluid inclusion data from the Zaaiplaats Sn field point to the occurrence of vapour- and liquid-rich fluid inclusions demonstrating that boiling promoted precipitation of cassiterite and associated minerals (Pollard et al., 1991). A boiling mechanism is essentially associated with a drop in fluid pressure. In the case of the Zaaiplaats Sn field, a combination of decreasing temperatures and increasing fluid volumes led to phase separation and hydro-fracturing, which resulted in hydrothermal breccias and pipes. Explosion-breccias are documented from multiple hydrothermal pipes across the Zaaiplaats Sn field (Strauss, 1954), which likely reflect a boiling event. The structurally-controlled Rooiberg and Union Sn fields represent infiltrations of the ore-bearing fluids into the Transvaal Supergroup and the volcaniclastic horizons of the Rooiberg Group, respectively. Rozendaal et al. (1995) related the hydrothermal brecciation associated with the Rooiberg Sn field to a volatile-rich fluid overpressure enriched in CO_2, as inferred by the carbonate-dominated matrix, and fluid boiling induced by the associated rapid pressure release.

In line with the fluid boiling scenario, Nazari-Dehkordi and Robb (2022b) identified irregular REE patterns in hydrothermal zircons associated with the Zaaiplaats Sn field that mirror those reported from cassiterite in this study, providing further support for the preferential partitioning of trace elements into the liquid and vapour phases. Therefore, the compositional variations of, and the redox states recorded by, the cassiterites from various Bushveld Sn fields likely depended ultimately on the presence of co-existing phases that formed alongside or immediately before cassiterite and had the ability to fractionate incompatible elements. Moreover, fluid-rock interactions, particularly in the case of the exogranitic Sn fields, resulted in compositional changes, increasing oxygen fugacity and lowering temperatures (Rozendaal et al., 1995). In the Zaaiplaats Sn field, the cassiterite ores are accompanied by numerous minerals such as zircon, apatite, tourmaline, fluorite, scheelite, bastnaesite and synchysite (Pollard et al., 1991; McNaughton et al., 1993). This ore mineral assemblage derived from a volatile-rich fluid with markedly high concentrations of incompatible elements such as Zr, Hf, Nb and Ta. The relative depletion of the endogranitic cassiterites in a number of elements such as U, Th, REE, W, Fe, Ti and Mn (Figs. 7, 8, 10) are likely due to an early separation of phosphates, scheelite and ilmenite, while a relative enrichment of In is because of a lack of associated sulphides as preferred hosts of In (Pavlova et al., 2015). In the case of the exogranitic Rooiberg and Union Sn fields, the ore mineral assemblages are surrounded by a halo of alteration assemblages representing sericitisation, chloritisation and silicification that compositionally modified and variably increased the oxygen fugacity of the ore-bearing granitic fluids. These exogranitic Sn fields comparatively represent lower degrees of fractionation, as indicated by cassiterites with near-chondritic Zr/Hf ratios, and are depleted in HFSE-bearing minerals but contain abundant sulphides leading to low In values in the co-existing cassiterites.

6.4. Comparison with cassiterite from other localities

Most published compositional data for cassiterite come from the Bolivian Sn belt (Gemmrich et al., 2021) and the South China Block (Guo et al., 2018; Cheng et al., 2019; Liu et al., 2021). Tin mineralisation in the Bolivian Sn belt is hosted mainly within sedimentary successions spatially related to two episodes of felsic magmatism aged ~218 Ma and ~24 Ma (Gemmrich et al., 2021). Cassiterite compositions have been reported from nine exogranitic Sn-bearing districts of the Bolivian Sn belt (n = 245, Gemmrich et al., 2021). Similarly, Sn mineralisation associated with the Longxianggai Granite (~96 Ma, Guo et al., 2018) from the Dachang (n = 106, Guo et al., 2018) and Dulong (n = 75, Liu et al., 2021) districts of the South China Block is also exogranitic, whereas the Sn ore reported from the Gejiu district, as documented in Cheng et al. (2019), appears as both endogranitic (granite-hosted and greisen ores, n = 53) and exogranitic (skarn, semi-oxidised, oxidised and vein-type ores, n = 69). Moreover, chemical compositions of endogranitic cassiterites are available for a number of rare-metal granites and pegmatites. Feng et al. (2019) documented cassiterite compositions (n = 41) from the ~220 Ma Kangxiwa-Dahongliutan pegmatite field, Western Kunlun Orogen, China, containing significant amounts of Sn, W, Be, Li,

Nb and Ta. Greisen-type mineralisation within the highly differentiated ~155 Ma Maoping granite, Gannan metallogenic belt, South China Block, contains notable cassiterite ore (n = 33) associated with monazite, apatite, topaz and Li mica (Chen et al., 2019). Furthermore, Nambaje et al. (2020) recorded compositional variations of cassiterite ore (n = 53) from the ~980 Ma Rwinkwavu pegmatites of the Karagwe Ankole Sn-Nb-Ta-W metallogenic belt of Rwanda.

A comparison between cassiterite mineral compositions from the Zaaiplaats, Union and Rooiberg Sn fields with the published dataset from the above-mentioned localities shows that the data points from the intrusive-distal Sn ores of the Bolivian Sn belt and those from the South China Block straddle a trend defining a Zr/Hf ratio of 40 analogous to those reported in this study from the exogranitic Union and Rooiberg Sn fields. By contrast, the endogranitic Zaaiplaats Sn field defines a Zr/Hf ratio of ~10 that is comparable to similar ores reported from the South China Block (Fig. 12). However, endogranitic cassiterite ores reported from rare-metal pegmatites are distinctly enriched in Zr and Hf, and appear along a trend with a Zr/Hf ratio of ~3. Notably, the exogranitic Union and Rooiberg Sn fields share a similar Zr/Hf ratio with barren or poorly-mineralised granitic bodies that are defined by Zr/Hf ratios of 30–50 (average Zr/Hf = 40; Ballouard et al., 2016), corresponding to the Charge-and-Radius-Controlled (CHARAC) field of Bau (1996), where the distribution of Zr, Hf and other trace elements is governed exclusively by ionic radius and charge. The endogranitic cassiterites exhibit two distinct trends with Zr/Hf ratios of ~10 and ~3, which share non-CHARAC Zr/Hf ratios with variably mineralised granites (Ballouard et al., 2016). The Zr/Hf ratios of ~10, exhibited by the Zaaiplaats Sn field, are usually characteristic of granite-hosted Sn—W deposits, whereas extremely low Zr/Hf ratios (Zr/Hf = ~3) are associated with highly fractionated rare-metal granites and pegmatites containing substantial quantities of Li, Cs, Ta, Nb, Be, Sn and W (Ballouard et al., 2016). Trace element behaviour within the non-CHARAC field is governed largely by chemical complexation with a wide variety of species such as H_2O, F, B and Cl that are abundant in highly evolved high-silica magmatic rocks (Bau, 1996).

Collectively, the existing mineral compositional datasets that define endogranitic and exogranitic cassiterites from around the world, although limited, appear to readily distinguish their environment and genesis on the basis of Zr and Hf contents. The Zr versus Hf discrimination diagram may thus be useful in distinguishing the endogranitic and exogranitic origins of detrital cassiterites and in identifying the extent to which the causative source is fractionated.

7. Conclusion

The major findings of this study include:

1. Representative cassiterite samples from both endogranitic (Zaaiplaats) and exogranitic (Rooiberg and Union) Sn deposits yielded ages that overlap with those reported from the Bushveld LIP.
2. The Bushveld Sn fields have remained largely unaffected by post-Bushveld magmatic and hydrothermal activities, further confirming that conventional isotopic dating techniques can be applied to Paleoproterozoic cassiterites.
3. Trace element compositions of the endogranitic and exogranitic cassiterites from the Bushveld LIP are consistent with derivation from a granitic source.
4. Compositional variations of the endogranitic and exogranitic cassiterites resulted from the co-existing phases with the ability to fractionate trace elements and, in the case of the exogranitic cassiterites, also from extensive fluid-rock interactions.
5. The endogranitic and exogranitic cassiterite samples, although sharing comparable REE patterns, develop compositionally distinct trends. In particular, exogranitic cassiterites are defined by Zr/Hf ratios of ~40, whereas endogranitic cassiterites reported from the Zaaiplaats Sn field have lower Zr/Hf ratios of ~10 that are nevertheless higher than those reported from endogranitic cassiterites associated with rare-metal granites and pegmatites (Zr/Hf = ~3).

CRediT authorship contribution statement

Teimoor Nazari-Dehkordi: Conceptualisation; Field investigations; Software; Visualization; Data Curation; Writing - Original Draft, Writing - Review and Editing.

Xiao-Lei Wang: Formal analysis; Writing - Original Draft; Writing - Review and Editing.

Axel Hofmann: Supervision; Conceptualisation; Field investigations; Writing - Original Draft; Writing - Review and Editing.

Rong-Qing Zhang: Formal analysis; Writing - Original Draft, Writing - Review and Editing.

Laurence Robb: Supervision; Conceptualisation; Field investigations; Writing - Original Draft; Writing - Review and Editing.

Henriette Ueckermann: Formal analysis; Writing - Original Draft; Writing - Review and Editing.

Declaration of competing interest

The authors declare that they have no known competing financial

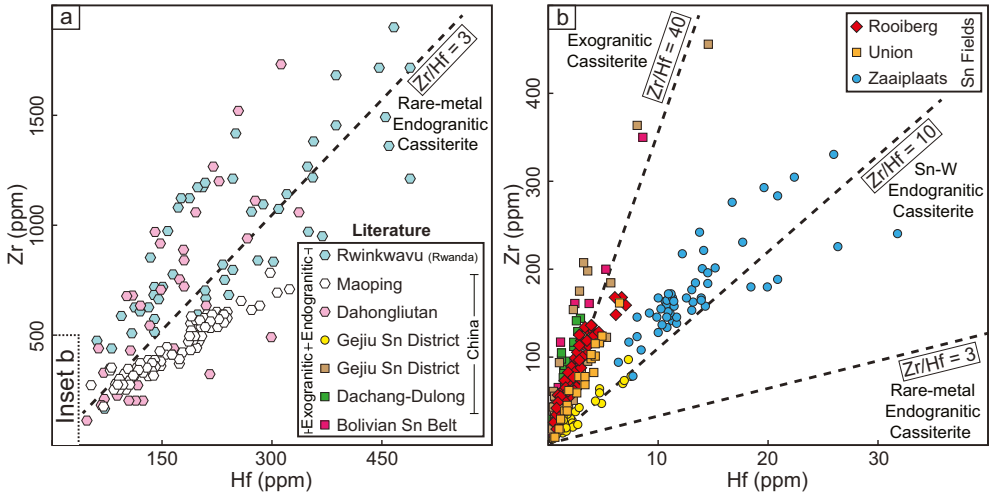

Fig. 12. Discrimination diagram of Zr (ppm) versus Hf (ppm) for the Zaaiplaats, Union and Rooiberg Sn fields (n = 182) showing that exogranitic cassiterite data points are defined by Zr/Hf of ~40, whereas endogranitic cassiterite samples define two trends one with Zr/Hf of ~10 associated with Sn—W granites and another one with Zr/Hf of ~3 related to rare-metal granites and pegmatites. Note that cassiterites from rare-metal granites and pegmatites are remarkably rich in Zr and Hf. Data sources (n = 675): Bolivian Sn belt (n = 245): Gemmrich et al. (2021); Dachang (n = 106): Guo et al. (2018); Dulong (n = 75): Liu et al. (2021); and Gejiu Sn district (n = 122): Cheng et al. (2019); Dahongliutan pegmatite (n = 41): Feng et al. (2019); Maoping granite (n = 33): Chen et al. (2019); Rwinkwavu pegmatite, Rwanda (n = 53): Nambaje et al. (2020).

interests or personal relationships that could have appeared to influence the work reported in this paper.

Data availability

Data analysed in this article are included in the supplementary materials.

Acknowledgments

Special thanks to Ben Cohen, Jade Greve, Timothy Marais and Marina Yudovskaya for helping with fieldwork, to Schalk Krugel for providing access and sampling permission, to Ding-Yi Xiong for cassiterite U-Pb isotopic analysis, and to Bennon Development Company (Leeuwpoort Quarry) and AfriTin Mining Ltd. for providing logistical support. The manuscript greatly benefited from extensive reviews by two anonymous reviewers and from editorial handling of Stefano Albanese. The support of the DSI-NRF Centre of Excellence (CoE) for Integrated Mineral and Energy Resource Analysis (DSI-NRF CIMERA) towards this research is acknowledged.

Appendices. Supplementary data

Supplementary data to this article can be found online at https://doi.org/10.1016/j.gexplo.2023.107310.

References

Ballouard, C., Poujol, M., Boulvais, P., Branquet, Y., Tartese, R., Vigneresse, J.-L., 2016. Nb-Ta fractionation in peraluminous granites: a marker of the magmatic-hydrothermal transition. Geology 44, 231–234. https://doi.org/10.1130/G37475.1.

Barnes, S.J., Maier, W.D., Curl, E.A., 2010. Composition of the marginal rocks and sills of the Rustenburg Layered Suite, Bushveld complex, South Africa: implications for the formation of the platinum-group element deposits. Econ. Geol. 105, 1491–1511. https://doi.org/10.2113/econgeo.105.8.1491.

Bau, M., 1996. Controls on the fractionation of isovalent trace elements in magmatic and aqueous systems: evidence from Y/Ho, Zr/Hf, and lanthanide tetrad effect. Contrib. Mineral. Petrol. 123, 323–333. https://doi.org/10.1007/s004100050159.

Boardman, L.G., 1946. The geology of a portion of the Rooiberg Tin fields. Trans. Geol. Soc. S. Afr. 49, 103–132.

Carr, P.A., Zink, S., Bennett, V.C., Norman, M.D., Amelin, Y., Blevin, P.L., 2020. A new method for U-Pb geochronology of cassiterite by ID-TIMS applied to the Mole Granite polymetallic system, eastern Australia. Chem. Geol. 539, 119539 https://doi.org/10.1016/j.chemgeo.2020.119539.

Cawthorn, R.G., Walraven, F., 1998. Emplacement and crystallization time for the Bushveld complex. J. Petrol. 39, 1669–1687. https://doi.org/10.1093/petroj/39.9.1669.

Cawthorn, R.G., Eales, H.V., Walraven, F., Uken, R., Watkeys, M.K., 2006. The Bushveld complex. In: Johnson, M.R., Anhaeusser, C.R., Thomas, R.J. (Eds.), The Geology of South Africa. Geological Society of South Africa.

Chen, L.L., Ni, P., Dai, B.Z., Li, W.S., Chi, Z., Pan, J.Y., 2019. The genetic association between Quartz Vein- and Greisen-Type mineralization at the Maoping W-Sn deposit, Southern Jiangxi, China: insights from Zircon and Cassiterite U-Pb ages and Cassiterite Trace Element Composition. Minerals 9, 411. https://doi.org/10.3390/min9070411.

Cheng, Y., Spandler, C., Kemp, A., Mao, J., Rusk, B., Hu, Y., Blake, K., 2019. Controls on cassiterite (SnO_2) crystallization: evidence from cathodoluminescence, trace-element chemistry, and geochronology at the Gejiu Tin District. Am. Mineral. 104, 118–129. https://doi.org/10.2138/am-2019-6466.

Coetzee, J., 1984. A Geochemical and Petrographical Investigation of the Low-Grade Tin Deposits in the Bobbejaankop Granite at the Zaaiplaats Tin Mine (Unpublished MSc thesis). University of Pretoria (137 pp).

Crocker, I.T., Eales, H.V., Ehlers, D.L., 2001. The Fluorite, Cassiterite and Sulphide Deposits Associated With the Acid Rocks of the Bushveld Complex, 80. Council for Geoscience, Pretoria, pp. 1–151.

De Waal, S.A., Armstrong, R.A., 2000. The age of the Marble Hall diorite, its relationship to the Uitkomst complex, and evidence for a new magma type associated with the Bushveld igneous event. S. Afr. J. Geol. 103, 128–140. https://doi.org/10.2113/103.2.128.

De Waal, S.A., Graham, I.T., Armstrong, R.A., 2006. The Lindeques drift and Heidelberg intrusions and the Roodekraal complex, Vredefort, South Africa: co-magmatic plutonic and volcanic products of a 2055 Ma ferro-basaltic magma. S. Afr. J. Geol. 109, 279–300. https://doi.org/10.2113/gssajg.109.3.279.

Feng, Y., Liang, T., Yang, X., Zhang, Z., Wang, Y., 2019. Chemical evolution of Nb-Ta oxides and cassiterite in phosphorus-rich albite-spodumene pegmatites in the Kangxiwa-Dahongliutan Pegmatite Field, Western Kunlun Orogen. China. Minerals 3, 166. https://doi.org/10.3390/min9030166.

Gemmrich, L., Torró, L., Melgarejo, J.C., Laurent, O., Vallance, J., Chelle-Michou, C., Sempere, T.P., 2021. Trace element composition and U-Pb ages of cassiterite from the Bolivian tin belt. Mineral. Deposita 56, 1491–1520. https://doi.org/10.1007/s00126-020-01030-3.

Gulson, B.L., Jones, M.T., 1992. Cassiterite: potential for direct dating of mineral deposits and a precise age for the Bushveld complex granites. Geology 20, 355–358. https://doi.org/10.1130/0091-7613(1992)020<0355:CPFDDO>2.3.CO;2.

Guo, J., Zhang, R., Sun, W., Ling, M., Hu, Y., Wu, K., Luo, M., Zhang, L., 2018. Genesis of tin-dominant polymetallic deposits in the Dachang district, South China: insights from cassiterite U-Pb ages and trace element compositions. Ore Geol. Rev. 95, 863–879. https://doi.org/10.1016/j.oregeorev.2018.03.023.

Haapala, I., 1997. Magmatic and post-magmatic processes in tin-mineralized granites: topaz-bearing leucogranite in the Eurajoki rapakivi granite stock, Finland. J. Petrol. 38, 1645–1659. https://doi.org/10.1093/petroj/38.12.1645.

Hamilton, J.M., Bishop, D.T., Morris, H.C., Owens, O.E., 1982. Geology of the Sullivan orebody, Kimberley, BC, Canada. In: Hutchinson, R.W., Spence, C.D., Franklin, J.M. (Eds.), Precambrian Sulphide Deposits, Geological Association of Canada Special Paper, vol. 25, pp. 597–665.

Heinrich, C.A., Eadington, P.J., 1986. Thermodynamic predictions of the hydrothermal chemistry of arsenic, and their significance for the paragenetic sequence of some cassiterite-arsenopyrite-base metal sulfide deposits. Econ. Geol. 81, 511–529. https://doi.org/10.2113/gsecongeo.81.3.511.

Hennigh, Q., Hutchison, R.W., 1999. Cassiterite at Kidd Creek: an example of volcanogenic massive sulfide-hosted tin mineralization. In: Hannington, M.D., Barrie, C.T. (Eds.), The Giant Kidd Creek Volcanogenic Massive Sulfide Deposit, Western Abitibi Subprovince, Canada, Economic Geology Monograph, vol. 10, pp. 431–440.

Hill, M., Barker, F., Hunter, D., Knight, R., 1996. Geochemical Characteristics and Origin of the Lebowa Granite Suite, Bushveld complex. Int. Geol. Rev. 38, 195–227. https://doi.org/10.1080/00206819709465331.

Hoskin, P.W.O., Schaltegger, U., 2003. The composition of zircon and igneous and metamorphic petrogenesis, in: Hanchar, J.M., Hoskin, P.W.O. (Eds.). Rev. Mineral. Geochem. 53, 27–62. https://doi.org/10.2113/0530027.

Hunter, D.R., 1975. The Regional Geological Setting of the Bushveld Complex. Economic Geology Research Unit, University of the Witwatersrand, Information Circular No. 96 (16 pp).

Kleemann, G.J., Twist, D., 1989. The compositionally-zoned sheet-like granite pluton of the Bushveld complex: evidence bearing on the nature of A-type magmatism. J. Petrol. 30, 1383–1414. https://doi.org/10.1093/petrology/30.6.1383.

Laurent, O., Rapopo, M., Stevens, G., Moyen, J.F., Martin, H., Doucelance, R., Bosq, C., 2014. Contrasting petrogenesis of Mg-K and Fe-K granitoids and implications for post-collisional magmatism: case study from the late-Archean Matok pluton (Pietersburg block, South Africa). Lithos 196, 131–149. https://doi.org/10.1016/j.lithos.2014.03.006.

Lenthall, D.H., 1974. Tin Production from the Bushveld Complex. Economic Geology Research Unit, University of the Witwatersrand, Information Circular No. 93 (25 pp).

Lerouge, C., Gloaguen, E., Wille, G., Bailly, L., 2017. Distribution of in and other rare metals in cassiterite and associated minerals in Sn±W ore deposits of the western Variscan Belt. Eur. J. Mineral. 29, 739–753. https://doi.org/10.1127/ejm/2017/0029-2673.

Leube, A., Stumpfl, E.F., 1963. The Rooiberg and Leeuwpoort tin mines, Transvaal, South Africa. Econ. Geol. 58, 527–557. https://doi.org/10.2113/gsecongeo.58.3.391.

Linnen, R.L., 1998. The solubility of Nb-Ta-Zr-Hf-W in granitic melt with Li and Li+F: constraints for mineralization in rare metal granite and pegmatite. Econ. Geol. 93, 1013–1025. https://doi.org/10.2113/gsecongeo.93.7.1013.

Liu, S., Liu, Y., Ye, L., Wei, C., Cai, Y., Chen, W., 2021. Genesis of dulong Sn-Zn-In polymetallic deposit in Yunnan Province, South China: insights from cassiterite U-Pb ages and trace element compositions. Minerals 11, 199. https://doi.org/10.3390/min11020199.

Losos, Z., Beran, A., 2004. OH defects in cassiterite. Mineral. Petrol. 81, 219–234. https://doi.org/10.1007/s00710-004-0040-x.

Maier, W., Prevec, S., Scoates, Wall, C.J., Barnes, S.J., Gomwe, T., 2018. The Uitkomst intrusion and Nkomati Ni-Cu-Cr-PGE deposit, South Africa: trace element geochemistry, Nd isotopes and high-precision geochronology. Mineral. Deposita 53, 67–88. https://doi.org/10.1007/s00126-017-0716-x.

Mathez, E.A., VanTongeren, J.A., Schweitzer, J., 2013. On the relationships between the Bushveld complex and its felsic roof rocks, part 1: petrogenesis of Rooiberg and related fesites. Contrib. Mineral. Petrol. 166, 435–449. https://doi.org/10.1007/s00410-013-0884-3.

McDonald, I., Tredoux, M., Vaughan, D.J., 1995. Platinum mineralization in quartz veins near Naboomspruit, central Transvaal. S. Afr. J. Geol. 98, 168–175.

McNaughton, N.J., Pollard, P.J., Groves, D.I., Taylor, R.G., 1993. A long-lived hydrothermal system in Bushveld granites at the Zaaiplaats tin mine: Lead isotope evidence. Econ. Geol. 88, 27–43. https://doi.org/10.2113/gsecongeo.88.1.27.

Menge, G.F.W., 1963. The Cassiterite Deposits on Doornhoek 342 KR and Vicinity, West of Naboomspruit, Transvaal (Unpublished MSc thesis). University of the Witwatersrand (74 pp).

Möller, P., Dulski, P., Szacki, W., Malow, G., Riedel, E., 1988. Substitution of tin in cassiterite by tantalum, niobium, tungsten, iron and manganese. Geochim. Cosmochim. Acta 52, 1497–1503. https://doi.org/10.1016/0016-7037(88)90220-7.

Monecke, T., Kempe, U., Trinkler, M., Thomas, R., Dulski, P., Wagner, T., 2011. Unusual rare earth element fractionation in a tin-bearing magmatic-hydrothermal system. Geology 39, 295–298. https://doi.org/10.1130/G31659.1.

Murciego, A., Sanchez, A.G., Dusausoy, Y., Pozas, J.M.M., Ruck, R., 1997. Geochemistry and EPR of cassiterites from the Iberian Hercynian Massif. Mineral. Mag. 61, 357–365. https://doi.org/10.1180/minmag.1997.061.406.03.

Nambaje, C., Eggins, S.M., Yaxley, G.M., Sajeev, K., 2020. Micro-characterisation of cassiterite by geology, texture and zonation: a case study of the Karagwe Ankole Belt, Rwanda. Ore Geol. Rev. 124, 103609 https://doi.org/10.1016/j.oregeorev.2020.103609.

Nambaje, C., Williams, I.S., Sajeev, K., 2021. SHRIMP U-Pb dating of cassiterite: insights into the timing of Rwandan tin mineralisation and associated tectonic processes. Ore Geol. Rev. 135, 104185 https://doi.org/10.1016/j.oregeorev.2021.104185.

Nazari-Dehkordi, T., Robb, L., 2022a. Geochemical constraints on the origin and evolution of the volcanic Rooiberg Group, Bushveld Large Igneous Province, South Africa. Precambrian Res. 369, 106509 https://doi.org/10.1016/j.precamres.2021.106509.

Nazari-Dehkordi, T., Robb, L., 2022b. Zircon mineral chemistry and implications for magmatic-hydrothermal evolution of the granite-hosted Zaaiplaats Sn deposit, Bushveld Large Igneous Province, South Africa. Lithos 416-417, 106672. https://doi.org/10.1016/j.lithos.2022.106672.

Nazari-Dehkordi, T., Huizenga, J.M., Spandler, C., Oliver, N.H.S., 2019. Fluid inclusion and stable isotope constraints on the heavy rare earth element mineralisation in the Browns Range Dome, Tanami Region, Western Australia. Ore Geol. Rev. 113, 103068 https://doi.org/10.1016/j.oregeorev.2019.103068.

Neymark, L.A., Holm-Denoma, C.S., Moscati, R.J., 2018. In situ LA-ICPMS U-Pb dating of cassiterite without a known-age matrix-matched reference material: examples from worldwide tin deposits spanning the Proterozoic to the Tertiary. Chem. Geol. 483, 410–425. https://doi.org/10.1016/j.chemgeo.2018.03.008.

Neymark, L.A., Holm-Denoma, C.S., Larin, A.M., Moscati, R.J., Plotkina, Y.Y., 2021. LA-ICPMS U-Pb dating reveals cassiterite inheritance in the Yazov granite, Eastern Siberia: implications for tin mineralization. Mineral. Deposita 56, 1177–1194. https://doi.org/10.1007/s00126-020-01038-9.

Oliveira, J.T., Pacheco, N., Carvalho, P., Ferreira, A., 1997. The Neves Corvo mine and the Paleozoic geology of Southwest Portugal. In: Barriga, F.J.A.S., Carvalho, D. (Eds.), Geology and VMS Deposits of the Iberian Pyrite Belt, SEG Neves Corvo Field Conference 1997, Guidebook Series 27, pp. 21–71. https://doi.org/10.5382/GB.27.02.

Olsson, J.R., Söderlund, U., Klausen, M.B., Ernst, R.E., 2010. U-Pb baddeleyite ages linking major Archean dyke swarms to volcanic-rift 1882 forming events in the Kaapvaal craton (South Africa), and a precise age for the Bushveld complex. Precambrian Res. 183, 490–500. https://doi.org/10.1016/j.precamres.2010.07.009.

Pavlova, G.G., Palessky, S.V., Borisenko, A.S., Vladimirov, A.G., Seifert, T., Phan, L.A., 2015. Indium in cassiterite and ores of tin deposits. Ore Geol. Rev. 66, 99–113. https://doi.org/10.1016/j.oregeorev.2014.10.009.

Pollard, P.J., Taylor, R.G., Tate, N.M., 1989. Textural evidence for quartz and feldspar dissolution as a mechanism of formation for Maggs Pipe, Zaaiplaats tin mine, South Africa. Mineral. Deposita 24, 210–218. https://doi.org/10.1007/BF00206444.

Pollard, P.J., Andrew, A.S., Taylor, R.G., 1991. Fluid inclusion and stable isotope evidence for interaction between granites and magmatic hydrothermal fluids during formation of disseminated and pipe-style mineralization at the Zaaiplaats tin mine. Econ. Geol. 86, 121–141. https://doi.org/10.2113/gsecongeo.86.1.121.

Rajesh, H.M., Chisonga, B.C., Shindo, K., Beukes, N.J., Armstrong, R.A., 2013. Petrographic, geochemical and SHRIMP U-Pb titanite age characterization of the Thabazimbi mafic sills: extended timeframe and a unifying petrogenetic model for the Bushveld Large Igneous Province. Precambrian Res. 230, 79–102. https://doi.org/10.1016/j.precamres.2013.02.002.

Robb, L.J., Robb, V.M., Walraven, F., 1994. The Albert Silver Mine revisited: towards a model for polymetallic mineralization in granites of the Bushveld complex, South Africa. Explor. Min. Geol. 3, 247–262.

Robb, L.J., Freeman, L.A., Armstrong, R.A., 2000. Nature and longevity of hydrothermal fluid flow and mineralisation in granites of the Bushveld complex, South Africa. Earth Environ. Sci. Trans. R. Soc. Edinb. 91, 269–281. https://doi.org/10.1017/S0263593300007434.

Rozendaal, A., Misiewicz, J.E., Scheepers, R., 1995. The tin zone: sediment-hosted hydrothermal tin mineralization at Rooiberg, South Africa. Mineral. Deposita 30, 178–187. https://doi.org/10.1007/BF00189347.

Rubin, J.N., Henry, C.D., Price, J.G., 1993. The mobility of zirconium and other immobile elements during hydrothermal alteration. Chem. Geol. 110, 29–47. https://doi.org/10.1016/0009-2541(93)90246-F.

Schaltegger, U., Pettke, T., Audetat, A., Reusser, E., Heinrich, C.A., 2005. Magmatic-to-hydrothermal crystallization in the W-Sn mineralized mole granite (NSW, Australia) - part I: crystallization of zircon and REE-phosphates over three million years - a geochemical and U-Pb geochronological study. Chem. Geol. 220, 215–235. https://doi.org/10.1016/j.chemgeo.2005.02.018.

Schweitzer, J.K., Hatton, C.J., De Waal, S.A., 1995. Regional lithochemical stratigraphy of the Rooiberg Group, upper Transvaal Supergroup; a proposed new subdivision. S. Afr. J. Geol. 98, 245–255.

Scoates, J.S., Wall, C.J., Friedman, R.M., Weis, D., Mathez, E.A., VanTongeren, J.A., 2021. Dating the Bushveld complex: timing of crystallization, duration of magmatism, and cooling of the world's largest layered intrusion and related rocks. J. Petrol. 62, egaa107 https://doi.org/10.1093/petrology/egaa107.

Sharpe, M.R., 1981. The chronology of magma influxes to the eastern compartment of the Bushveld complex as exemplified by its marginal border groups. J. Geol. Soc. Lond. 138, 307–326.

Shmulovich, K., Heinrich, W., Möller, P., Dulski, P., 2002. Experimental determination of REE fractionation between liquid and vapour in the systems NaCl-H_2O and $CaCl_2$–H_2O up to 450 °C. Contrib. Mineral. Petrol. 144, 257–273. https://doi.org/10.1007/s00410-002-0397-y.

Skursch, O., Tegner, C., Lesher, C.E., Cawthorn, R.G., 2020. Two expressions of the transition from mafic cumulates to granitoids in the Bushveld complex, South Africa: examples from the western and eastern limbs. Lithos 372-373, 105671. https://doi.org/10.1016/j.lithos.2020.105671.

Strauss, C.A., 1947. Granitization and rheomorphism associated with the granite near the Leeuwpoort tin mine. Trans. Geol. Soc. S. Afr. 50, 161–170.

Strauss, C.A., 1954. The geology and mineral deposits of the Potgietersrus tin fields. South Afr. Geol. Surv. Mem. 46, 241.

Tapster, S., Bright, J.W., 2020. High-precision ID-TIMS cassiterite U–Pb systematics using a low-contamination hydrothermal decomposition: implications for LA-ICP-MS and ore deposit geochronology. Geochronology 2, 425–441. https://doi.org/10.5194/gchron-2-425-2020.

Taylor, S.R., McLennan, S.M., 1985. The Continental Crust: Its Com Position and Evolution. Blackwell, Oxford.

Tindle, A.G., Breaks, F.W., 1998. Oxide minerals of the Separation Rapids rare-element granitic pegmatite group, north-western Ontario. Can. Mineral. 36, 609–635.

Van Achterbergh, E., Ryan, C.G., Jackson, S.E., Griffin, W.L., 2001. Data reduction software for LA-ICP-MS. In: Sylvester, P.J. (Ed.), Laser Ablation-ICP Mass Spectrometry in the Earth Sciences: Principles and Applications, Mining Association of Canada, vol. 29, pp. 239–243.

Walraven, F., 1985. Genetic aspects of the granophyric rocks of the Bushveld complex. Econ. Geol. 80, 1166–1180. https://doi.org/10.2113/gsecongeo.80.4.1166.

Walraven, F., 1987. Textural, geochemical and genetic aspects of the granophyric rocks of the Bushveld complex. South Afr. Geol. Surv. Mem. 72, 145.

Walraven, F., 1997. Geochronology of the Rooiberg Group, Transvaal Supergroup, South Africa. Economic Geology Research Unit, University of the Witwatersrand, Information Circular No 316 (20 pp).

Wu, F.Y., Yang, Y.H., Li, Q.L., Mitchell, R.H., Dawson, J.B., Brandl, G., Yuhara, M., 2011. In situ determination of U-Pb ages and Sr-Nd-Hf isotopic constraints on the petrogenesis of the Phalaborwa carbonatite complex, South Africa. Lithos 127, 309–322. https://doi.org/10.1016/j.lithos.2011.09.005.

Zeh, A., Ovtcharova, M., Wilson, A.H., Schaltegger, U., 2015. The Bushveld complex was emplaced and cooled in less than one million years-results of zirconology, and geotectonic implications. Earth Planet. Sci. Lett. 418, 103–114. https://doi.org/10.1016/j.epsl.2015.02.035.

Zhang, R.Q., Lehmann, B., Seltmann, R., Sun, W.D., Li, C.Y., 2017a. Cassiterite U-Pb geochronology constrains magmatic-hydrothermal evolution in complex evolved granite systems: the classic Erzgebirge tin province (Saxony and Bohemia). Geology 45, 1095–1098. https://doi.org/10.1130/G39634.1.

Zhang, R.Q., Lu, J.J., Lehmann, B., Li, C.Y., Li, G.L., Zhang, L.P., Guo, J., Sun, W.D., 2017b. Combined zircon and cassiterite U-Pb dating of the Piaotang granite-related tungsten-tin deposit, southern Jiangxi tungsten district, China. Ore Geol. Rev. 82, 268–284. https://doi.org/10.1016/j.oregeorev.2016.10.039.

Zirakparvar, A.N., Mathez, E.A., Rajesh, H.M., Choe, S., 2019. Lu-Hf isotopic evidence of a deep mantle plume source for the ~2.06 Ga Bushveld Large Igneous Province. Lithos 348-349, 105168. https://doi.org/10.1016/j.lithos.2019.105168.